Thermo-regenerable supramolecular host-guest inclusion complex of randomly methylated β-cyclodextrin with polymerized ionic liquid as energy-efficient draw solutes in forward osmosis

Hana G. Zeweldi,[a†] Anelyn P. Bendoy, [a†] Myoung Jun Park,[b] Ho Kyong Shon,[b] Han-Seung Kim, [c]Eldin M. Johnson, [d,e] Hern Kim,[a] Wook-Jin Chung,[a*] Grace M. Nisola [a*]

[a] *Environmental Waste Recycle Institute (EWRI), Department of Energy Science and Technology (DEST), Myongji University, Myongji-ro 116, Cheoin-gu, Yongin-si, Gyeonggi-do 17058, Republic of Korea*

[b] *Center for Technology in Water and Wastewater, School of Civil and Environmental Engineering, University of Technology Sydney (UTS), Sydney MSW 2007, Australia*

[c] *Department of Environmental Engineering and Energy, Myongji University, Myongji-ro 116, Cheoin-gu, Yongin-si, Gyeonggi-do 17058, Republic of Korea*

[d] *Center for Nutraceutical and Pharmaceutical Materials, Myongji University, Yongin, Gyeonggi-do 17058, South Korea*

[e] *Department of Life Science, Food Microbiology and Bioprocess Laboratory, National Institute of Technology, Rourkela, India*

[†] Co-first authors

**Corresponding authors:*

(W.-J. Chung) wjc0828@gmail.com; (G.M. Nisola) grace.nisola@gmail.com;

Abstract

Supramolecular inclusion complexes with lower critical solution temperature (LCST) properties were investigated for the first time as draw solutes for forward osmosis (FO). Randomly methylated-β-cyclodextrin (Rm-β-CD) is employed as host for polymerized ionic liquids $([vbim]TFSI)_n$ with hydrophobic bis(trifluoromethylsulfonyl)imide anions ($TFSI^-$) as guest molecules. The LCST properties of Rm-β-CD/$([vbim]TFSI)_n$ were carefully tuned by varying the chain lengths of the guest PILs $([vbim]TFSI)_n$. Short-chain oligo([vbim]TSFI) with MW = 966.35 g mol^{-1} is the most suitable guest for Rm-β-CD. Prepared draw solutions (DS) from Rm-β-CD/ oligo([vbim]TSFI) exhibited highly tunable cloud-point temperatures (T_c), fast LCST kinetics and sufficient osmotic properties needed for an efficient FO operation. A 0.5 M Rm-β-CD/ 0.078 M oligo([vbim]TSFI) DS induced very competitive FO water flux (J_v ~ 13.725 ± 0.15 L $m^{-2}h^{-1}$) with negligible reverse solute flux (J_s ~ 4.41 × 10^{-3} $molm^{-2}h^{-1}$) against DI water as feed under PRO mode. It successfully desalinated 0.6 M NaCl FS with reasonable J_v ~ 4.33 ± 0.23 L $m^{-2}h^{-1}$, very low J_s ~ 0.0046 $molm^{-2}h^{-1}$, and superior J_s/J_V ~0.001 $molm^{-2}h^{-1}$, which highlights it potential for FO desalination. Rm-β-CD/oligo([vbim]TSFI) was efficiently recovered (~ 95%) by thermal precipitation with only 5°C temperature elevation (~ 30°C) from the FO operating temperature. Subsequently, trace DS was removed via nanofiltration (% SR~ 99.33) producing non-toxic water effluents. Results demonstrate the first supramolecular host-guest complexes as thermo-responsive draw solutes with energy-efficient recovery for long term application in FO membrane technology.

Keywords: *desalination; draw solution; forward osmosis; supramolecular; LCST; nanofiltration*

1. Introduction

Forward osmosis (FO) is gaining significant attention for desalination technology due to its potential as a less energy intensive alternative to reverse osmosis (RO) [1-3]. The water transport in FO is naturally driven by the osmotic pressure gradient ($\Delta\pi$) across a semi-permeable membrane, from a saline feed solution (FS) to a more concentrated draw solution (DS) [4,5]. Thus, unlike RO, FO does not require hydraulic pressure except for the circulation of the FS and DS [6-8].

To produce the final purified effluent and to recycle the DS, the draw solutes are typically recovered from the spent DS for re-use. However, this step is energy-intensive especially when conventional inorganic salts (i.e. NH_3/CO_2, NaCl, $MgCl_2$, $CaCl_2$, $NaHCO_3$, KBr, K_2SO_4) [9, 10], organic compounds (i.e. hydroacid complexes, zwitterions, ethylenediamine tetraproponic salt, polyelectrolytes) [11-15], and ionic liquids (i.e. 2-methyimidazole based diodide [16], [N2222]Br [17], and 1-Sodium acetate-2,3-dimethyl imidazolium iodide [18]) are used. Their recovery often requires processes like evaporation [19,20], distillation [21], reverse osmosis (RO) [9], nanofiltraion (NF) [22], and membrane distillation (MD) [16,17]. Thus, while FO alone is energy-efficient [23,24], the subsequent solute regeneration step amplifies the total energy requirement, making it less competitive with RO [23-25].

Recent developments have focused on reducing the energy requirements for draw solute recovery by employing "smart" materials like magnetic nanoparticles (MNPs) [26], CO_2-responsive [27], and thermo-responsive compounds (i.e. ionic liquids, morpholines, copolymers, polymers, hydrogels, glycol ethers) [28-34]. Their ability to respond to external stimuli is exploited for their separation from water. But so far, magnetization of MNPs and heating of CO_2-responsive and thermo-responsive materials still consume high energy [8, 10; 19, 26, 27, 35- 37] thus, remains a challenge.

One sensible approach towards energy-efficient recovery is to modulate the responsive behavior of the draw solutes towards the stimulus. Thermo-responsiveness offers this option as draw solutes with lower critical solution temperature (LCST) can have different cloud-point temperatures (T_c), which dictate the condition at which thermal precipitation (TP) and separation from water occur. So far, LCST-type FO draw solutes with T_c ~ 28 ºC – 70ºC like BuMP [30], PSSS-PINIPAM [35], PNiPAM-SA [14], PSSP11 [32], P($MT_{20}EO_{80}$) [34], [N4444]2,4,6-$MeSO_3$ [36], [P444]TsO [37], GE_7B_3 [38], and PNA-10 [39] have been reported but were heated at T = 45 ºC – 70 ºC to maximize their precipitation or recovery efficiency [14, 30, 32, 34-39]. This indicates that the TP temperature must be at least ΔT ~ 20 ºC above FO temperature, equivalent to a heat energy requirement of E_{TP} ~ 23 kWh m^{-3} ($E_{TP} = mc_p\Delta T/V$; m = mass of DS, V = volume of produced water, water specific heat capacity at 25ºC ~ c_p = 4.18 J g^{-1} ºC) that still far exceeds that of RO ~ 2-10 kWh m^{-3} [35,40,41]. Thus, it is imperative for an LCST draw solute to have high de-mixing efficiency so that the TP temperature is operated only slightly above its T_c. Moreover, a lower T_c would reduce ΔT and in effect, the E_{TP}.

Apart from recovery issues, majority of the reported LCST draw solutes have inferior FO performances with unknown toxicity profiles [14. 30, 35, 38, 39]. Thus, it remains of utmost importance to develop and employ LCST draw solutes whose properties are tuned not only for their feasible TP recovery but also for their competitive FO performance (i.e. high water flux or J_w, negligible reverse solute diffusion or $\underline{J_s}$) and non-toxicity for safe consumption [7, 27, 29, 36, 37].

Among the prospective draw solutes, cyclodextrins (CDs) are cyclic oligosaccharides with truncated cone-like structures and outer surface rich in C_6 primary -OH groups, which render them hydrophilic, water-soluble, and capable of generating osmotic pressure [43-46]. Meanwhile, the

hydrophobic inner cavities of CDs are attractive hosts for various hydrophobic guest compounds like poly(caprolactone) [47], α-amino acid [48], Poly(lactide-co-glycolide)[49], Poly(methacrylamides) [50], and adamantane [60] . Their capability to form host-guest inclusion complexes has been proven useful for sustained release of hydrophobic drugs with CDs acting as osmotic agents [46, 52-54]. Their biocompatibility has rendered them safe and highly useful in various areas like pharmaceuticals [55], food [56], cosmetics [57], textile industry [58], and bioconversions [59]. Such salient features suggest the potential of CDs as ideal draw solutes.

In pure solutions, CDs have no LCST properties but previous works have shown their pseudo-LCST behavior with imidazolium-based hydrophobic polymerized ionic liquids (PILs) as guest molecules [61,62]. The LCST behavior is based on a thermo-reversible CD/PIL complexation and de-complexation mechanism, hence, can be tuned to facilitate an efficient TP recovery process. Furthermore, ILs are also attractive draw solutes due to their excellent thermal stability, low toxicity, and good ionic properties which could aid in the osmotic property of the DS [16,17,28,29,45]. Thus, the combined benefits of CDs and PILs as CD/PIL host-guest complexes can be exploited to develop draw solutes with efficient FO performance and TP recovery.

This study reports the first FO draw solute of CD/polymerized IL as host-guest complexes with LCST properties. Random methylated β-CD (Rm-β-CD) was used as host for hydrophobic PIL – 1-vinyl-3-butyl-imidazolium bis(trifluoromethylsulfonyl)imide or $([vbim]TFSI)_n$ (Scheme 1a). The wide rim (d = 1.5 nm) of Rm-β-CD can easily accommodate the hydrophobic anion component $TFSI^-$ of $([vbim]TFSI)_n$, which has an approximate size of 0.39 nm [44, 61, 62].

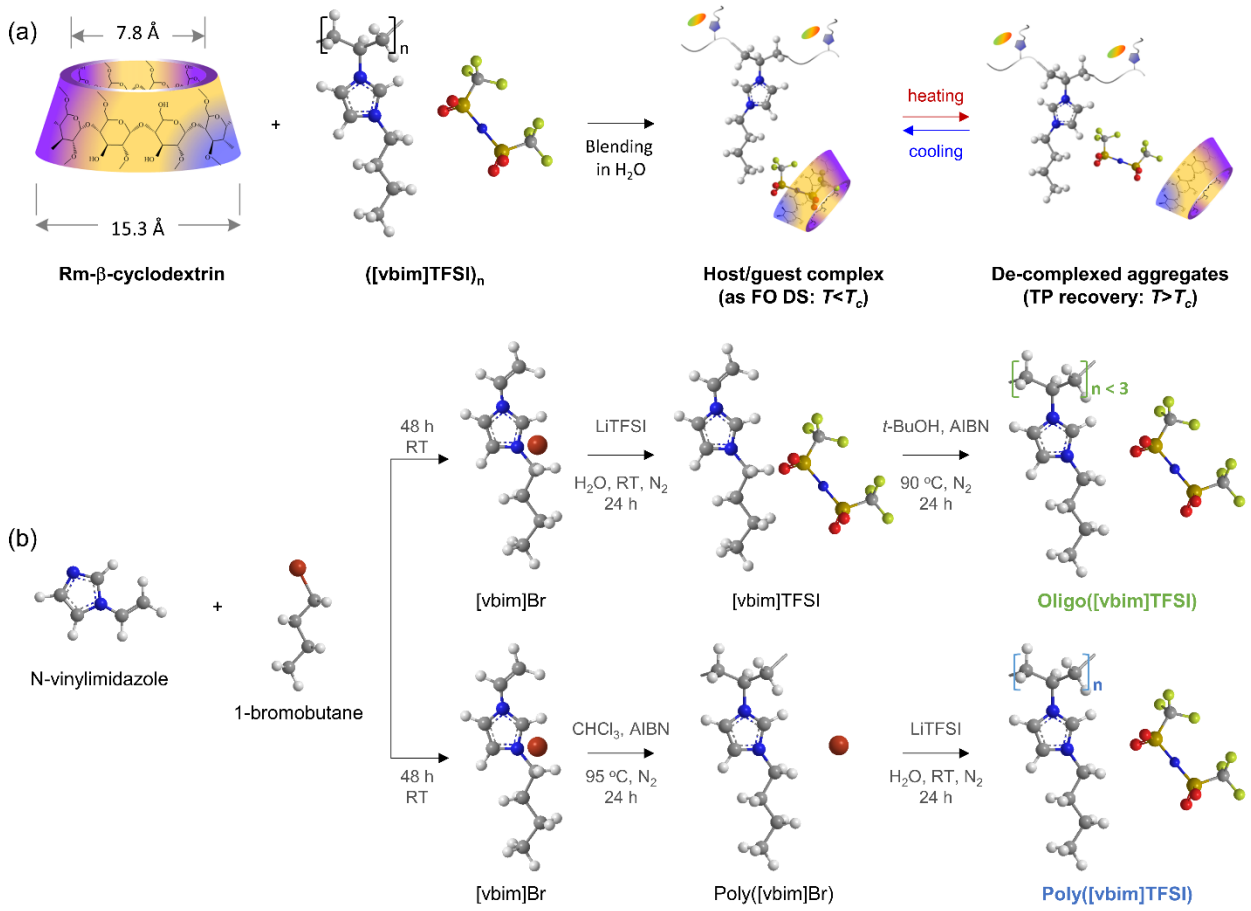

Scheme 1. (a) Rm-β-CD/([vbim]TFSI)$_n$ as supramolecular host/guest FO draw solutes with LCST properties. (b) Synthetic routes for PILs ([vbim]TFSI)$_n$ with different chain lengths route 1 for oligo([vbim]TFSI) and route 2 for poly([vbim]TFSI).

Their suitability as draw solutes were initially assessed in terms of their colligative- and physico-chemical properties. Meanwhile, their LCST properties were carefully tuned by varying the chain lengths of ([vbim]TFSI)$_n$, their molar ratios with Rm-β-CD/([vbim]TFSI)$_n$ and concentrations of Rm-β-CD/([vbim]TFSI)$_n$ to achieve the lowest T_c possible. Their performance as FO DS was investigated using deionized water (DI) and simulated seawater solution (0.6 M NaCl) as feed to evaluate their potential application for desalination. After FO, TP was carried out to recover the

bulk Rm-β-CD/([vbim]TFSI)$_n$ and finally, nanofiltration (NF) was employed as a final step for high quality effluent production and residual draw solutes removal. The operation was carried out in cycles to demonstrate the reusability of Rm-β-CD/([vbim]TFSI)$_n$. The biocompatibility and safety of Rm-β-CD/([vbim]TFSI)$_n$ was evaluated through *in vitro* toxicity tests. Finally, energy consumption of FO-NF with TP for bulk Rm-β-CD/([vbim]TFSI)$_n$ recovery was estimated and compared with other reported DS and with RO.

2. Materials and Methods

2.1. Materials

Methylated-*β*-cyclodextrin (Rm-β-CD) was procured from Tokyo Chemicals Industry Co., Ltd. (Japan). Other purchased materials for PIL ([vbim]TFSI)$_n$ synthesis, DS characterization, and water analysis for FO runs are listed in supplementary information (SI p. S4). All chemicals were used without further purification unless otherwise stated.

2.2. Synthesis of PILs ([vbim]TFSI)$_n$ and Rm-β-CD/([vbim]TFSI)$_n$ DS preparation

The reactions for PIL ([vbim]TFSI)$_n$ synthesis are shown in **Scheme 1b**, which initially involve preparation of intermediate [vbim]Br by mixing equimolar amounts of 1-bromobutane and vinylimidazole in an ice bath for 20 min then at room temperature (RT) for 48 h **[**60, 61, 63**]**. The product was washed thrice each with diethyl ether and ethyl acetate, then vacuum-dried at RT to obtain a colorless viscous liquid [vbim]Br. Two synthesis routes were subsequently carried out depending on the degree of polymerization (*n*). Three types of ([vbim]TFSI)$_n$ ILs were prepared with varied chain lengths. For route 1, short-chain oligo([vbim]TFSI) IL was prepared through: (1) ion exchange between [vbim]Br and LiTFSI in DI water to afford an orange viscous liquid

[vbim]TFSI followed by (2) radical its polymerization in *tert*-butyl alcohol with AIBN initiator. For route 2, two long-chain poly([vbim]TFSI) ILs were synthesized in opposite sequence: (1) radical polymerization of [vbim]Br in chloroform ($CHCl_3$) with AIBN initiator to afford poly([vbim]Br) [63] then (2) its ion exchange with LiTFSI in DI water. Two types of poly([vbim]TFSI) with different *n* repeating units were obtained from route 2 by varying the amount of AIBN initiator. Purification of oligo([vbim]TFSI) and long-chain poly([vbim]TFSI) were similar as discussed in detail in SI p. S5. All PILs were vacuum-dried in at 60°C then stored in dry environment when not in use. Details of $([vbim]TFSI)_n$ synthesis including amounts of reactant used and reaction conditions were provided in SI p. S5. Draw solutions of Rm-β-CD/$([vbim]TFSI)_n$ were prepared by mixing different types of $([vbim]TFSI)_n$ and Rm-*β*-CD (i.e. at varied molar ratios and concentrations) in DI water at RT.

2.3. Structural properties of draw solutes

The successful preparation of oligo- and poly([vbim]TFSI) was confirmed through Fourier transform infrared (FTIR) spectroscopy (Varian Scimitar FTIR 2000, USA) at RT using standard attenuated total reflection (FTIR-ATR) method. Their chemical structures were further confirmed using Fourier transform nuclear magnetic resonance analysis (Varian, 400 MR FT-NMR, USA). Prior NMR ^{1}H (400 MHz) and ^{13}C (100 MHz) spectra acquisition, intermediates [vbim]Br, [vbim]TFSI and poly([vbim]Br) were dissolved in deuterated chloroform ($CDCl_3$) whereas the final $([vbim]TFSI)_n$ products were prepared in dimethyl sulfoxide (DMSO). Average molecular weights (M_w), number average molecular weight (M_n), and polydispersity index (*PDI*) were determined by gel permeation chromatography (Agilent 1100 series GPC) with refractive index detector. The samples were dissolved in tetrahydrofuran (THF) at 1 g L^{-1}, injected (20 µL) with THF as the eluent (1 mL min^{-1}) through the PL gel 10 µm MIXED-B column (23°C) [64].

2.4. Physico-chemical properties of draw solutes

Bulk diffusion coefficients (D_{aq}) of Rm-β-CD, [vbim]TFSI monomer and ([vbim]TFSI)$_n$ samples were estimated using Wilke-Chang correlation [65]. Meanwhile, the molar volume (V_m) of the solutes at their normal boiling point (V_b) were estimated using Tyn and Calus correlation [66]. The critical volume (V_c) was determined using the extended Lydersen-Joback-Reid group contribution method [67]. Details of the calculation of D, V_b, and V_c are provided in **SI p. S6.**

Osmolalities of pure Rm-β-CD and selected Rm-β-CD/([vbim]TFSI)$_n$ were measured against the osmolality calibration curves of standard NaCl solution (**SI Fig S1**) at varied concentrations (0.1 – 2 M) with corresponding freezing point depressions as detailed in **SI p. S7** [46, 68]. Dynamic scanning calorimetry (DSC 3, Mettler Toledo, Switzerland) was used to measure the melting or freezing point of samples frozen at -50°C then gradually heated to 30 °C at 5°C min^{-1}. Viscosities (η) were determined using a viscometer (DV-II + BROOKFIELD®, USA) with a rotating spindle speed of 100 rpm. Ionic strengths (I) were calculated from the conductivity (κ) measurements (LAQUA act, Horiba Scientific, Japan) through Russell's relationship [16] as shown in Eq. (1):

$$I = \kappa(\mu S/cm) \times 1.6 \times 10^{-5} \quad (1)$$

2.5. Thermal properties of draw solutes and DS

Thermal decomposition pure Rm-β-CD and Rm-β-CD/([vbim]TFSI)$_n$ were recorded on a thermo-gravimetric analyzer (TGA Mettler Toledo, DSC823e, South Korea) from 30^{o}C to 800^{o}C at 10^{o}C min^{-1} in N_2 (flow rate: 50 mL min^{-1}). Their LCST properties were probed by determining their T_c using UV-Vis spectrophotometer (Agilent 8453, USA) equipped with a temperature controller (Quantum Northwest, USA). The samples were dissolved in DI water and their % transmittances

were measured at λ=560 nm while being heated from 25°C – 70°C at 1ºC min^{-1}. LCST kinetics of selected Rm-β-CD/([vbim]TFSI)$_n$ were also investigated [69], as detailed in **SI., p. S8**. Careful tuning of the T_c value was carried out by observing the effects of ([vbim]TFSI)$_n$ chain length, Rm-β-CD/([vbim]TFSI)$_n$ molar ratios and Rm-β-CD/([vbim]TFSI)$_n$ concentration. The specific heat capacity (c_p) of selected DS was also measured from transformed heat flow DSC curve of the DS [70]. The change in hydrodynamic diameter (D_h) of the draw solutes during heating was monitored by dynamic light scattering (DLS) technique using Zetasizer Nano ZS (Malvern, South Korea). Particle size expressed as apparent Z-average hydrodynamic diameter was measured at back scattering angle of 173º with a He/Ne laser (λ = 633 nm) at 25 – 70ºC. Each measurement was done in triplicates and data was reported as average of the three measurements.

2.6. FO performance using Rm-β-CD/([vbim]TFSI)$_n$ DS

FO experiments were performed on a laboratory-scale crossflow set-up (**Fig. 1a**) with a membrane cell 7.7 cm long × 2.6 cm wide × 0.3 cm deep [17]. A commercially available thin film composite membrane (TFC) from a disassembled spiral wound CSM FO 4040 (Toray Industry Korea Inc., South Korea) was used in all FO runs. The membrane is ~100 μm thick with a polyamide (PA) active layer on a porous polysulfone (PSf) support. The PA surface has a contact angle of 48.36 ± 5.8 º while the support has 69.78 ± 1.77 º. The membrane was stored at 4 ºC in DI water and was equilibrated for 30 min at RT before use. The FS V = 500 mL and DS V = 100 mL were circulated by gear pumps (Cole-Parmer, USA) at 0.4 L min^{-1} (cross flow velocity = 8.55 cm s^{-1}) and maintained at 25 ± 1 ºC. A digital balance (AND® company limited, Japan) was used to monitor the weight gain in the DS reservoir, recorded by a data logger (AD-1688, AND® company limited, Japan). The FO setup was operated by placing the active PA layer of the membrane in contact with

either the FS (AL-FS or FO mode) or DS (AL-DS or PRO mode).

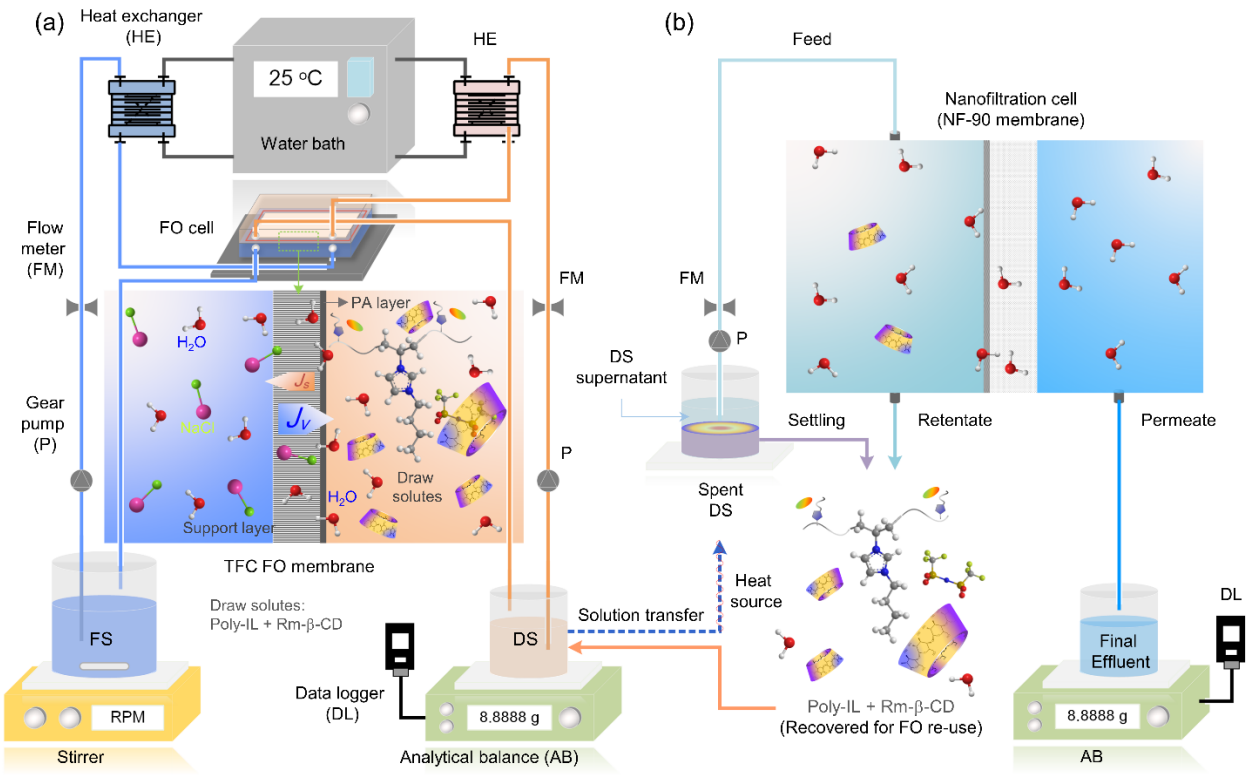

Fig. 1 Schematic representation of the (a) FO setup (AL-DS or PRO mode as depicted, and AL-FS or FO mode with reversed membrane orientation); and (b) subsequent TP for bulk Rm-β-CD/([vbim]TFSI)$_n$ and NF system for residual draw solute removal.

Water flux (J_v, L m^{-2} h^{-1}, LMH) was determined (Eq. 2) from the change in mass of the DS (Δm) at time interval (Δt), with known density of water (ρ_w) and effective membrane area $S_m \sim 20$ cm^2. Meanwhile, reverse solute flux (J_s, mol m^{-2}h^{-1}) was estimated (Eq. 3) from the FS solute concentration (C_t) and volume (V_t) at t, where FS $V_t = V_{t=0} - V_{\text{perm at } t} - V_{tot\_\text{sample}}$ where $V_{t=0} = 500$ mL, $V_{perm\ at\ t}$ is the volume of permeated water to DS and V_{tot_sample} is the accumulated volume loss due to sampling for C_t. The C_t values were measured using TOC analysis (TOC analyzer ASI-50000A, Shimadzu, Japan). A TOC calibration curve of different DS concentrations was used for C_t quantification. Specific reverse salt flux (J_s/J_v) of the DS was determined to estimate the draw

solute leakage during FO operation. The potential of Rm-β-CD/([vbim]TFSI)$_n$ for desalination application was assessed using simulated seawater (0.6 M NaCl) as FS.

$$J_v = \frac{\Delta m}{S_m \Delta t \rho_w} \quad (2)$$

$$J_s = \frac{\Delta (C_t V_t)}{S_m \Delta t} \quad (3)$$

2.7. Draw solute recovery

After each FO run, the spent DS is heated above its T_c to recover the bulk of Rm-β-CD/([vbim]TFSI)$_n$ through TP (**Fig. 1b**). The precipitate was allowed to settle to be separated from bulk water phase (DS supernatant). Liquid samples were analyzed using TOC to determine the draw solute concentrations in the spent DS (C_b) before TP and residual concentrations (C_s) in the DS supernatant after TP. The percentage recovery (%R) of the draw solutes (Eq. 4) was calculated from these measured concentrations [29,34].

$$R(\%) = \left(\frac{C_b - C_s}{C_b}\right) \times 100\% \quad (4)$$

The DS supernatant was subsequently fed in NF system to remove the trace draw solutes. The NF membrane employed is a 145 μm thick NF-90 membrane (Toray Industry Korea Inc., South Korea). This membrane has 98% rejection (NaCl) and water permeability of 1.10 ± 0.08 L m^{-2} h^{-1} bar^{-1} [36]. Dry NF-90 membrane was soaked in DI water overnight before use. The membrane (S_m = 9.075 cm^2) was fixed in a circular cross-flow filtration unit with diameter ∅ = 3.4 cm and depth h = 2 cm (cross flow velocity ~ 3.2 cm s^{-1}). Prior each run, NF system was pre-stabilized for 30 min with DI water as feed at 10 bars, actual operation was carried out at 10 bars and 25 ± 1 °C. NF

water flux (J_w) was calculated (Eq. 5) from the change in mass of permeated water (Δm) at Δt. Meanwhile, NF rejection efficiency (% *SR*) was estimated (Eq. 6) from the NF permeate concentration of the draw solute (C_p) and C_s as the DS supernatant was used as feed.

$$J_w = \frac{\Delta m}{S_m \Delta t \rho_w} \tag{5}$$

$$SR(\%) = (1 - \frac{C_p}{C_s}) \times 100 \tag{6}$$

2.8. Draw solute toxicity test

The toxicity of Rm-β-CD/([vbim]TFSI)$_n$ was investigated using human-derived colon carcinoma cells (Caco-2) with its culturing protocol described in **SI p. S9**. Viability assay was carried out by incubating the Caco-2 cells with Rm-β-CD/([vbim]TFSI)$_n$ at various concentrations (1 – 1000 mg L^{-1}) for 72 h in a CO_2 chamber. 3-(4,5-dimethylthiazol-2-yl)-2,5-diphenyltetrazolium bromide) (MTT) assay was used to measure cell viability [17]. Details of the protocol was provided in **SI p. S9 – S10**.

3. Results and Discussion

3.1. Physico-chemical properties

The M_w and volume properties (i.e. V_m, V_c and V_b) of Rm-β-CD (**Table 1**) reveal that it is a relatively large molecule with a D_{aq} similar with organic draw solutes GE_7B_3 and PEG1540 [38], but lower than smaller inorganic salts like NaCl, $MgCl_2$, and $CaCl_2$ [9]. Meanwhile, the M_w of PILs ([vbim]TFSI)$_n$ from GPC (**Table 1**) reveal their various chain lengths. Short-chain

oligo([vbim]TFSI) with M_w = 966.35 g mol^{-1} was successfully formed via route 1 which initially involved [vbim]TFSI monomer formation followed by its polymerization (**Scheme 1**). The bulky $TFSI^-$ anion in [vbim]TFSI monomers likely caused severe steric hindrance, which lessened the exposure of the vinyl moieties to the radicals thereby reducing the degree of polymerization [71,72]. Moreover, the low rate of monomer coupling at the propagation stage or the strong columbic interactions in [vbim]TFSI also inhibited the formation of high M_w ILs [71,72]. Reversal of the synthesis steps (route 2) afforded longer chains of Poly([vbim]TFSI) with $M_w = 8.95 \times 10^4$ g mol^{-1} (i.e. Poly([vbim]TFSI)-90K) and $M_w = 6.06 \times 10^6$ g mol^{-1} (i.e. Poly([vbim]TFSI)-6M) as [vbim]Br monomer is easier to polymerize than [vbim]TFSI in route 1. The longest $([vbim]TFSI)_n$ was obtained when at lower AIBN initatior. From the two routes, $([vbim]TFSI)_n$ ILs with different average chain lengths and repeating units n = 2.34 (oligo([vbim]TFSI), n = 207.32 (Poly([vbim]TFSI)- 90K) and $n = 1.4 \times 10^4$ (Poly([vbim]TFSI)-6M) were successfully obtained with $PDI \sim 1.55 – 3.50$. The D_{aq} of oligo([vbim]TFSI is similar with Rm-β-CD since they have similar molecular size and volume properties while the longer PILs Poly([vbim]TFSI)-90K and Poly([vbim]TFSI)-6M have significantly lower D_{aq}.

Table 1. Characterization of the draw solutions components at 25°C.

Compound	M_W [a] (g mol^{-1})	M_n [b] (g mol^{-1})	PDI [c]	n [d]	V_m [e] (cm^3 mol^{-1})	V_c [f] (cm^3 mol^{-1})	V_b [g] (cm^3 mol^{-1})	D_{aq} [h] (× 10^{-12} m^2 s^{-1})
Rm-β-CD	1,303.30	-	-	-	814.60	3,552.00	1,499.00	211
[vbim]TFSI	431.40	-	-	-	317.18	889.87	351.35	503
Oligo([vbim]TFSI)	966.35	623.21	1.55	2.34	709.82	2,526.58	1,048.80	261
Poly([vbim]TFSI)-90K	8.95×10^4	2.56×10^4	3.50	207.32	6.58×10^4	2.35×10^5	1.21×10^5	15
Poly([vbim]TFSI)-6M	6.06×10^6	3.92×10^6	1.55	1.40×10^4	4.46×10^6	5.49×10^7	3.68×10^7	0.49

[a] M_W – molecular weight; [b] M_n – number average molecular weights; [c] PDI–polydispersity index ; [d] n-degree of polymerization; [e] V_m – molar volume of solute at room temperature estimated from molecular weight/density; [f] V_c – critical volume of solute ; [g] V_b – is the molar volume (cm^3 mol^{-1}) of solute at its normal boiling temperature calculated using Tyn and Calus correlation; [h] D_{aq} – bulk diffusion coefficient calculated using Wilke-Chang method.

3.2. Structural characterization

The purchased Rm-β-CD is known to have ~57% of its –O-H groups randomly substituted with –CH_3 groups. Its FTIR signals (**Fig. 2a**) display all expected peaks from the O-H stretching at 3548-3239 cm^{-1}, C-H stretching at 2934 – 2939 cm^{-1} and bending at 1460 cm^{-1}, C-O-C stretching at 1159 cm^{-1} and C-O or C-C stretching at 1044 cm^{-1} (SI Table S1). Meanwhile, the synthesis of different $([vbim]TFSI)_n$ PILs: oligo([vbim]TFSI) poly([vbim]TFSI)-90K, and poly([vbim]TFSI)-6M were carefully monitored through FTIR after each reaction to ensure successful preparation (**Fig. 2a**). The FTIR spectra of intermediates [vbim]Br, poly[vbim]Br and [vbim]TFSI, and all PILs commonly feature the signals for the imidazolium ring: sp^2 C-H stretching at 3151-3087 cm^{-1}, sp^3 C-H stretching of the imidazole and alkyl chains at 2957 – 2870 cm^{-1}, C=C stretching at 1555-1570 cm^{-1}, and C-N stretching at 1156 cm^{-1} [60, 61, 63]. Anion exchange between [vbim]Br and LiTFSI was confirmed by the appearance of bond stretchings O=S=O at 1343 cm^{-1}, C-F at 1170 cm^{-1}, S-N-S at 1032 cm^{-1}, C-S at 787 cm^{-1} and S-N at 743 cm^{-1} in [vbim]TFSI [60, 61, 63]. Meanwhile, successful polymerization of [vbim]Br was proved by the weakened C=C intensity at ~ 1638 cm^{-1}. Finally, all PILs $([vbim]TFSI)_n$: oligo([vbim]TFSI) poly([vbim]TFSI)-90K, and poly([vbim]TFSI)-6M feature the expected spectra with reduced C=C stretching at 1650 cm^{-1} due to consumption of the vinyl diene during polymerization and presence of peaks related with imidazolium cation and exchanged $TFSI^-$ anion as mentioned above. The FTIR signals for each sample were also summarized in detail in **SI Table S1** [61, 63].

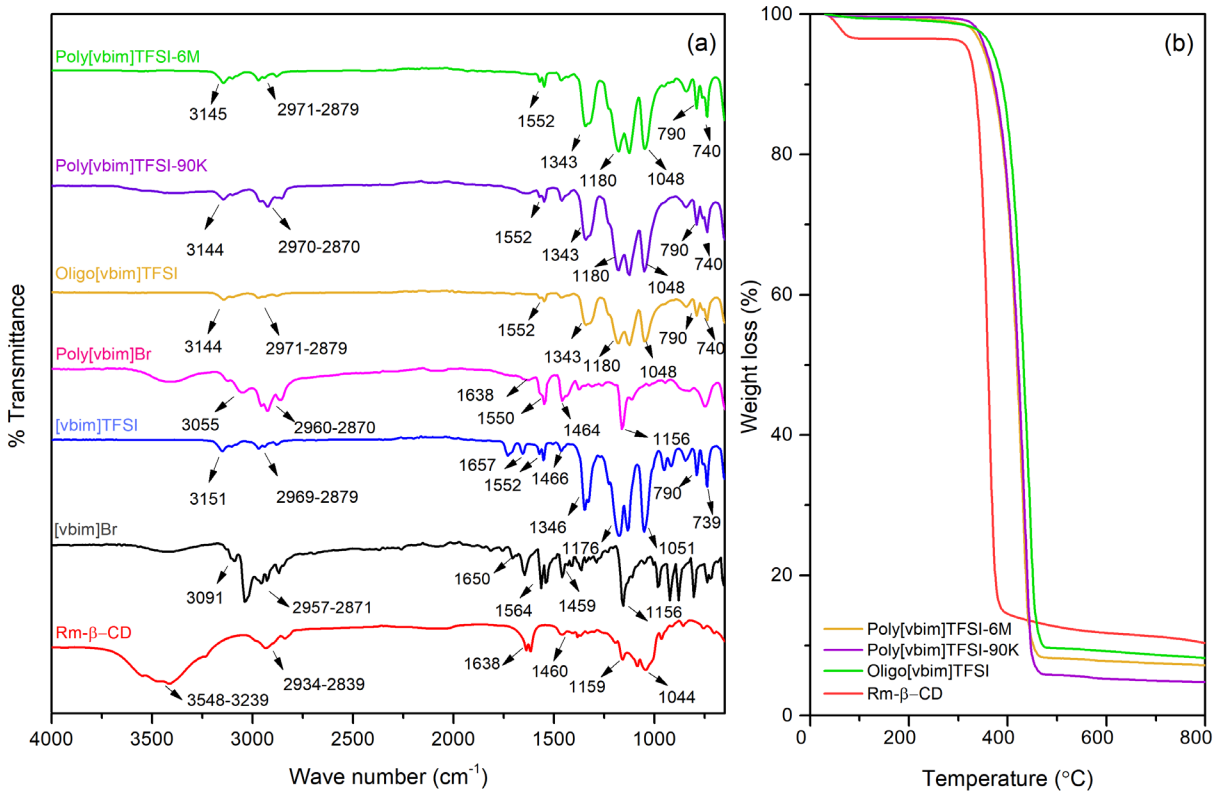

Fig. 2. (a) FTIR spectra of Rm-β-CD, [vbim]Br, [vbim]TFSI, poly[vbim]Br, oligo([vbim]TFSI), poly[vbim]TFSI-90K, and poly[vbim]TFSI-6M; (b) TGA curves of neat Rm-β-CD, oligo([vbim]TFSI), poly[vbim]TFSI-90K, and poly[vbim]TFSI-6M.

Given the overlapping FTIR signals, the chemical structures of [vbim]Br **(SI Fig. S2)**, [vbim]TFSI **(SI Fig. S3)** and PILs (**SI Figs. S4-S6)** were further confirmed by FT-NMR analysis. After polymerization, the chemical shifts for the vinyl protons of the monomers at 5.31, 5.41, and 5.90 ppm (**SI Figs. S2-S3**) completely disappeared and new signals corresponding to the polymeric backbone appeared at 2.19 and 4.34 ppm for oligo([vbim]TFSI) (**SI Fig. S4**), poly([vbim]TFSI)-90K (**SI Fig. S5**), and poly([vbim]TFSI)-6M (**SI Fig. S6**) indicating their successful preparation [61, 63].

3.3. Thermal behavior of Rm-β-CD and ([vbim]TFSI)$_n$

The thermal degradation curves of Rm-β-CD and synthesized ([vbim]TFSI)$_n$ ILs confirm that they are suitable draw solutes as they can be employed under elevated temperature conditions without decomposition (**Fig. 2b**). All neat samples are thermally stable with minimal mass loss at 100ºC due to residual moisture removal. Decomposition regions occurred at ~310 – 390ºC for Rm-β-CD and ~ 360ºC – 450ºC for the PILs, which are significantly higher than the needed temperatures for FO operation (T ~ 25ºC) and TP recovery (T < 100ºC).

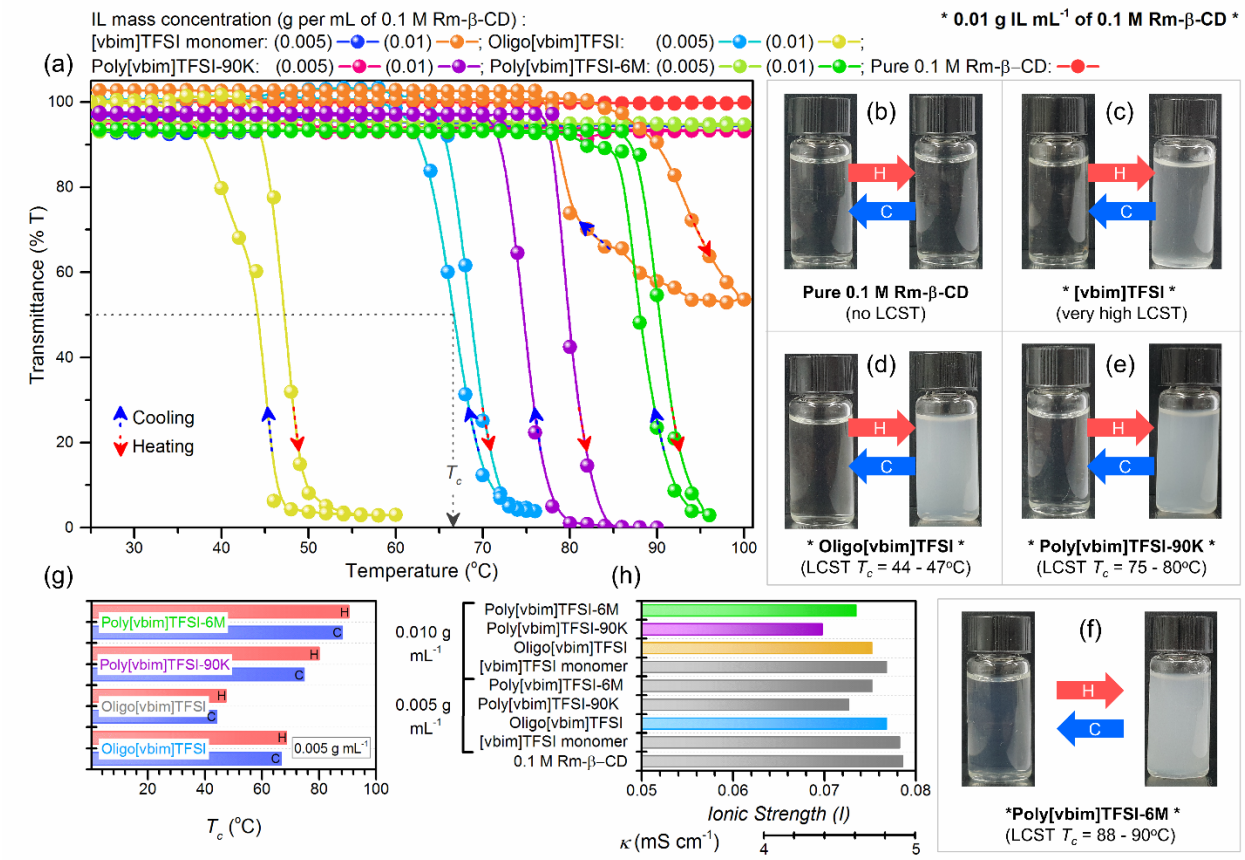

Fig. 3. (a) Transmittance of pure Rm-β-CD (0.1 M), 0.005 g mL^{-1} of [vbim]TFSI in 0.1M Rm-β-CD, 0.01g mL^{-1} of [vbim]TFSI in 0.1 M Rm-β-CD, 0.005 g mL^{-1} of oligo([vbim]TFSI) in 0.1M Rm-β-CD, 0.01g mL^{-1} of oligo[vbim]TFSI in 0.1M Rm-β-CD, 0.005g mL^{-1} of poly([vbim]TFSI)-90K in 0.1 M Rm-β-CD, 0.01 g mL^{-1} of poly([vbim]TFSI)-90K in 0.1M Rm-β-CD, 0.005g of poly([vbim]TFSI)-6M in 0.1 M Rm-β-CD, and 0.01g of poly([vbim]TFSI)-6M

in 0.1M Rm-β-CD during heating and cooling; visual illustration of reversible phase transition property: (b) pure Rm-β-CD (0.1M); and 0.01 g mL^{-1} of ILs in 0.1 M Rm-β-CD: (c) [vbim]TFSI; (d) oligo([vbim]TFSI); (e) poly([vbim]TFSI)-90K ; (f) poly([vbim]TFSI)-6M; (g) cloud point temperature (T_c) of 0.01 g mL^{-1} of ILs in 0.1 M Rm-β-CD during heating and cooling; (h) ionic strength and conductivity (k) of pure Rm-β-CD (0.1 M), 0.005 g mL^{-1} ILs in 0.1 M Rm-β-CD, and 0.01 g mL^{-1} ILs in 0.1 M Rm-β-CD.

The LCST properties of Rm-β-CD/([vbim]TFSI)$_n$ pairs were assessed from their transmittance (%T) curves under gradual heating (H) and cooling (C) at 1°C min^{-1}. Analysis of pure IL solutions is not possible because of their hydrophobicity and negligible solubility in water without the Rm-β-CD. Meanwhile, pure 0.1 M Rm-β-CD consistently displayed ~100 %T, confirming the hydrophilicity of the host molecule without LCST property (**Fig. 3a – 3b**). To induce LCST behavior, 0.1 M Rm-β-CD was added with each type of ([vbim]TFSI)$_n$ at fixed IL mass concentrations of 0.005 and 0.01 g mL^{-1}. At 25°C, all Rm-β-CD/IL solutions showed nearly ~100 %T. At this temperature, the ILs are rendered soluble in water as the complexation of $TFSI^-$ anion with Rm-β-CD breaks its ion pairing with $[vbim]^+$ cation [60]. Host-guest complexation of Rm-β-CD with the $TFSI^-$ is known to be an exothermic equilibration reaction [61]. Thus, increase in temperature will favor reactant formation or Rm-β-CD/IL de-complexation (**Scheme 1a**). The release of $TFSI^-$ anions from its Rm-β-CD host ensues precipitation, which becomes apparent when T_c is reached at 50 %T. Rm-β-CD/[vbim]TFSI monomer consistently displayed 100 %T at 0.005 g mL^{-1} and subtle turbidity at 0.01 g mL^{-1} (**Fig. 3c**), but its %T never reached 50% (**Fig. 3a).** The lack of LCST property of this pair indicates very high complex stability or strong affinity between the [vbim]TFSI monomer and Rm-β-CD, which cannot be disrupted by heat application to induce de-complexation [60,73].

In contrast, %T curves of Rm-β-CD/([vbim]TFSI)$_n$ pairs reveal LCST behaviors suggesting weaker complexation affinities between the host and the guest PILs. All phase transition is

reversible as %T reverted back to 100% with gradual cooling (C). Hysteresis between H and C curves exist due to the differences in complexation and de-complexation rates but have no effect on their reversible LCST behaviors. These results confirm that Rm-β-CD/([vbim]TFSI)$_n$ can be regenerated and re-used as FO DS through TP.

Variations in phase transition among the Rm-β-CD/([vbim]TFSI)$_n$ pairs can be seen in their %T curves **(Fig. 3a)**. Rm-β-CD/oligo([vbim]TFSI displayed LCST property even at low concentration (0.005 g mL^{-1}), which further occurred at lower temperatures **(Fig. 3d)** in doubled IL concentration (0.01 g mL^{-1}). Meanwhile, solutions with longer chain ILs Rm-β-CD/poly([vbim]TFSI-90K (**Fig. 3e**) and Rm-β-CD/poly([vbim]TFSI-6M (**Fig. 3f**) only started to show LCST behavior at higher IL concentration (0.01 g mL^{-1}). Differences in molar ratio of the IL with respect to Rm-β-CD could explain the distinct phase transition behavior of each Rm-β-CD/([vbim]TFSI)$_n$ pair. At fixed IL mass concentration, the molar ratio of oligo([vbim]TFSI) with Rm-β-CD is the highest among the polymerized ILs as it has the lowest M_w. High proportion of the hydrophobic component (oligo([vbim]TFSI with respect to Rm-β-CD) favored de-complexation, resulting in LCST behavior at lower temperature. Thus, the T_c value of 0.1 M Rm-β-CD is lowest with oligo([vbim]TFSI) and highest with poly([vbim]TFSI)-6M (**Fig. 3g**).

Moreover, LCST kinetics likely contributed to the convenient phase transition of Rm-β-CD/oligo([vbim]TFSI). Heating curve time profiles reveal that Rm-β-CD/oligo([vbim]TFSI) has the fastest decline in %T among the Rm-β-CD/([vbim]TFSI)$_n$ pairs (**SI Fig. S7**). Model fitting with a three-parameter sigmoid equation (**SI p. S8**) confirmed that the de-complexation rate is fastest for Rm-β-CD/oligo([vbim]TFSI (k = -0.73 ± 0.106 min^{-1}) and slowest for poly([vbim]TFSI)-6M (k = -0.39 ± 0.033 min^{-1}) (**SI Table S2**). Short-chain IL oligo([vbim]TFSI)

is the most mobile (i.e. highest D_{aq}) among the polymerized ILs. Thus, it was able to complex and decomplex the fastest from Rm-β-CD. Ionic strength and conductivity measurements (**Fig. 3h**) conform with the observed kinetic trend. The least reduction in I and κ relative to pure Rm-β-CD was observed in Rm-β-CD/[vbim]TFSI monomer followed by oligo([vbim]TFSI), lastly by Poly([vbim]TFSI)-90K) and Poly([vbim]TFSI)-6M). This indicates that the mobility of smaller ILs like [vbim]TFSI monomer or oligo([vbim]TFSI) are less restricted than longer ILs upon complexation with Rm-β-CD. Therefore, they experience less reductions in I and κ [74,75].

As the monomeric IL lacks LCST property, polymerization of [vbim]TFSI is found critical to achieve a reversible LCST phase transition. However, the chain length must be controlled to maintain the I of Rm-β-CD/([vbim]TFSI)$_n$ to induce sufficient water permeation during FO and fast LCST kinetics to minimize E_{TP} for its bulk recovery. The best Rm-β-CD/IL pair must have a highly tunable T_c that is above the FO operating temperature to ensure that the Rm-β-CD/([vbim]TFSI) remains in complexed form and completely dissolved in water for maximum osmotic property. At the same time, the T_c must be sufficiently low to minimize E_{TP}. Among the three polymerized ILs, oligo([vbim]TFSI) provided the lowest T_c values (**Fig. 3g**) and the fastest LCST kinetics, thus, it will require the least E_{TP}. It also showed the least reduction in I and κ as draw solution (**Fig. 3g)**. Moreover, Rm-β-CD would require the least IL mass concentration of oligo([vbim]TFSI) to achieve LCST behavior. As the most suitable draw solution, Rm-β-CD/oligo([vbim]TFSI) was further optimized in terms of LCST property prior FO operation.

3.4. Tuning the properties of Rm-β-CD/oligo([vbim]TFSI)

At 0.01 g mL^{-1}, Rm-β-CD/oligo([vbim]TFSI) exhibited T_c = 44 – 47 °C (**Fig. 3g**) which is used to

approximate the minimum TP temperature. The approximate ΔT = 19 – 22 ºC is still high and therefore, must be tuned to minimize E_{TP}. To achieve this, T_c was further reduced by increasing the hydrophobic fraction in the DS or by increasing the oligo([vbim]TFSI) concentration in 0.1 M Rm-β-CD (**Fig. 4a**). Among the concentrations tested, 0.1 M Rm-β-CD/0.016M oligo([vbim]TFSI) registered the lowest T_c values ~ (C) 37 ºC – (H) 41ºC (**Fig. 4b**) that are still above the FO operating temperature. This composition was selected for further investigation as it reduced the ΔT = 12 ºC – 16 ºC.

Increase in DS concentration at fixed 0.1 M Rm-β-CD/0.016M oligo([vbim]TFSI) composition was carried out to maximize the driving force across the FO membrane. The highest allowable DS concentration is 0.5 M Rm-β-CD/0.078 M oligo([vbim]TFSI); further increase resulted in highly viscous DS that is difficult to employ in FO (**Fig. 4c**)**.** The range of DS concentrations also displayed sufficient ionic strengths comparable with 2-methyimidazole based diodide [16], [N2222]Br [17], [N444]2,4,6-$MeSO_3$ [36], and [P4444]TsO [37], which have been effectively used as FO draw solutes. The osmolality of Rm-β-CD/oligo([vbim]TFSI) was derived from the melting points of frozen DS samples measured via DSC (**SI. Fig. S1),** using frozen NaCl solutions as standards [46; 68]. Osmolality increased from 0.799 ± 0.68 osmol kg^{-1} to 6.913 ± 0.22 osmol kg^{-1} with DS concentration (**Fig. 4d**). This range is comparable with those of EDTP-Na [13], [P4444]TsO [37], PSSP5 [19], PSSBP8 [32], 1-Sodium propionate-2,3-dimethyl imidazolium iodide [18], [P4444]DMBS [29], and BuMP [30], indicating that Rm-β-CD/oligo([vbim]TFSI) can be an effective osmotic agent to drive the FO process. The osmolality at lowest DS concentration (**Fig. 4c**) with equivalent π = 29 bars, is comparable with that of 0.6 M NaCl, which is the approximate salt concentration in seawater. This implies that this concentration may not be sufficient to create the osmotic gradient needed for seawater desalination but may be suitable for

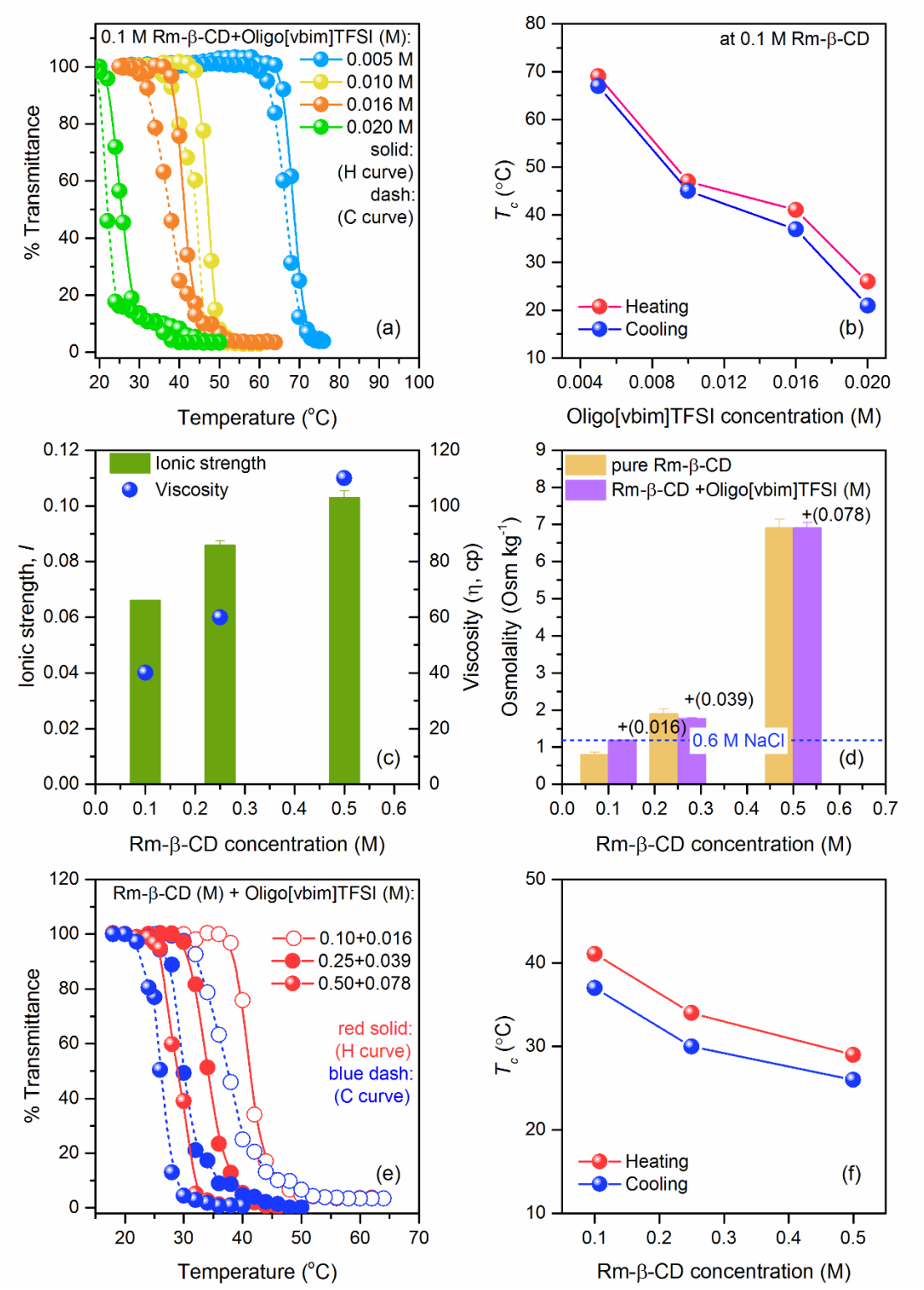

Fig. 4. **(a)** Reversible phase transition property of Rm-β-CD/oligo([vbim]TFSI) with 0.1 M Rm-β-CD at varied oligo([vbim]TFSI) concentration (0.005 – 0.02 M) ; (b) respective T_c values during heating and cooling (0.005 – 0.02 M); effect of Rm-β-CD/oligo([vbim]TFSI) concentration on

physico-chemical properties: (c) ionic strength and viscosity (η); (d) osmolality; (e) reversible phase transition property of Rm-β-CD/oligo([vbim]TFSI) at varied concentration (0.10 + 0.039 M), (0.25+0.078 M), and (0.50 + 0.078 M); and (f) respective T_c values during heating and cooling of Rm-β-CD/oligo([vbim]TFSI) at varied concentration (0.10 + 0.039 M), (0.25 + 0.078 M), and (0.50 + 0.078 M)

brackish water treatment ~ 0.15 M NaCl [29]. In contrast, the highest DS concentration registered the highest osmolality with equivalent π = 171.5 bars. Its high Δπ = relative to 0.6 NaCl (π = 27.6) suggests its potential for FO seawater desalination [76].

The phase transition behavior Rm-β-CD/oligo([vbim]TFSI) at varied concentrations was also examined to observe any changes in their LCST behavior. As shown, phase transition further shifted towards lower temperature with increase in DS concentration **(Fig. 4e).** The highest DS concentration registered T_c ~ 26ºC – 29ºC, which is still above the FO operating temperature. Considering the T_c value from H curve ~ 29ºC to mimic the scenario of heating the DS for TP, the ΔT has been significantly reduced to only ~ 4 ºC. So far, this is the lowest possible TP temperature reported in literature for LCST-type draw solutes and therefore, Rm-β-CD/oligo([vbim]TFSI) has the potential to require the lowest E_{TP} for its bulk recovery.

3.5 FO performance of Rm-β-CD/oligo([vbim]TFSI)

The ability of Rm-β-CD/oligo([vbim]TFSI) to induce water permeation as DS was confirmed through FO runs using DI water as feed under AL-FS (FO) and AL-DS (PRO) (**Fig. 5a and 5b**). Both modes of operation exhibit J_v increase, which can be related to the enhanced driving force ($\Delta\pi$) across the FO membrane affected by the osmolality increase with DS concentration. The J_v values under PRO mode are almost twice the J_v of FO. Under FO mode, dilutive internal concentration polarization (DICP) is prominent as the permeating water through the PA layer from the feed (Fig. 1) reduces the DS concentration at the support of the membrane [77-79]. As

relatively larger draw solutes, the lower D_{aq} of Rm-β-CD/oligo([vbim]TFSI) (i.e. than typical salts) likely exacerbated the DICP. In effect, the driving force is reduced resulting in remarkably lower J_v values under the FO mode. Compared with other reported DS (SI Table S3) also run in TFC FO membrane, the highest J_v induced by Rm-β-CD/oligo([vbim]TFSI) DS under PRO mode is higher than [N4444]2,4,6-$MeSO_3$ [36], [P4444]TsO [37], and PPG400 [38]. Rm-β-CD/oligo([vbim]TFSI) DS is likely competitive with [P4444]TMBS [29], [P4444]DMBS [16], NH_3-CO_2 [80], and $N(CH_3)_3$-CO_2 [81] since it was prepared at lower concentration. This demonstrates the potential of Rm-β-CD/oligo([vbim]TFSI) as draw solute in FO process.

The J_s was monitored to determine the extent of Rm-β-CD/oligo([vbim]TFSI) leakage towards the FS (**Fig. 5a and 5b**). In general, J_s values under both modes increased with the DS concentration. This indicates that reverse solute transport from the DS to the FS is enhanced by the proportional increase in the concentration gradient across the FO membrane [79]. The J_s values under FO mode were slightly lower than under PRO mode as the direct contact of the PA layer to the DS favored solute transport due to higher effective $\Delta\pi$ [77−79]. Nonetheless, the J_s values were extremely low even under PRO mode (~ 1.33 − 4.4 mmol $m^{-2}h^{-1}$) owing to the relatively larger size of Rm-β-CD and oligo([vbim]TFSI), which likely retarded their diffusion through the FO membrane. Other DS such as NH_3-CO_2 [80] and $N(CH_3)_3$-CO_2 [81] (**SI Table S3**) afforded higher J_v, but their J_s were also significantly higher than Rm-β-CD/oligo([vbim]TFSI). Moreover, other DS like PPG400 [38], [N4444]2,4,6-$MeSO_3$ [36], and [P4444]TsO [37] (**SI Table S3**) are less effective as they afforded lower J_v but higher J_s.

Consequently, competitive J_v and negligible J_s reflect the high FO efficiency of Rm-β-CD/oligo([vbim]TFSI) in terms of J_s/J_v, which estimates the mole of DS lost per volume of

permeated water. Results highlight the extremely low J_s/J_v ~ 0.26 − 0.32 mmol L^{-1} of Rm-β-CD/oligo([vbim]TFSI) especially under the PRO mode (**Fig. 5c-d**), which implies high membrane selectivity. This minimizes replenishment of the DS loss due to back transport through the FO membrane. Compared with other DS, the obtained J_s/J_v of Rm-β-CD/oligo([vbim]TFSI) in TFC FO membrane is comparable with PPG400 [38], [N4444]2,4,6-$MeSO_3$ [36], and [P4444]TsO [37], NH_3-CO_2 [80], $N(CH_3)_3$-CO_2 [81] and higher than [P4444]TMBS [29] and [P4444]DMBS [29] (**SI Table S3**).

For a broader literary comparison, FO was also operated at the highest DS concentration using the discontinued cellulose triacetate (CTA) FO membrane formerly produced by Hydration Technology Innovations (HTI, Albany, OR) [17]. This membrane was prominently used for DS testing in previous studies. Both J_v (10.75 L $m^{-2}h^{-1}$) and J_s (1. 56 mmol $m^{-2}h^{-1}$) values from CTA membrane were lower than the TFC membrane. But since the J_s was significantly lower, negligible J_s/J_v ~ 0.145 mmol L^{-1} of Rm-β-CD/oligo([vbim]TFSI) was obtained from the CTA membrane. Compared with reported DS tested in CTA, Rm-β-CD/oligo([vbim]TFSI) has lower J_s/J_v than inorganic salts [9, 80 − 82] and organic DS [16, 17, 77, 83 − 86] as detailed in **SI Table S3**. These values strongly support the competitive performance of Rm-β-CD/oligo([vbim]TFSI) as FO drawing agent.

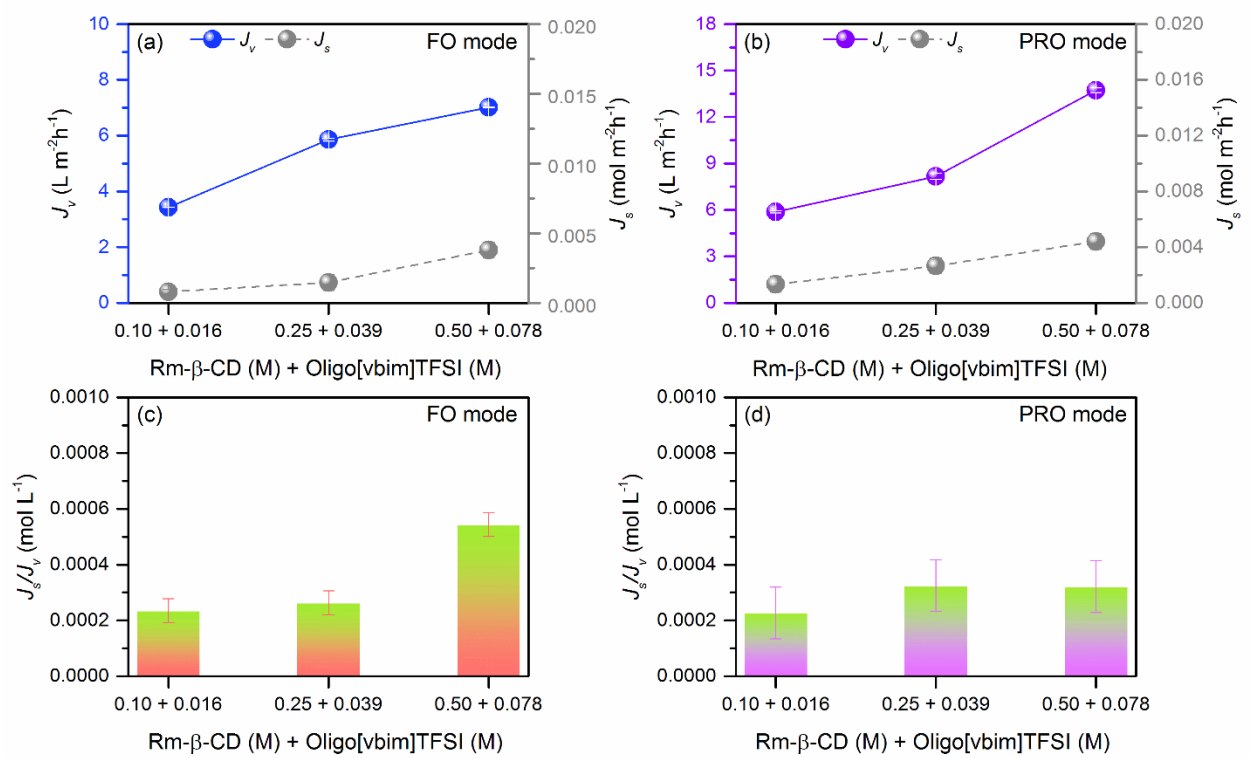

Fig. 5. FO performance of Rm-β-CD/oligo([vbim]TFSI) under FO and PRO mode (a) J_v and J_s in FO mode; (b) J_v and J_s in PRO mode; (c) J_s/J_v in FO mode; (d) J_s/J_v in PRO mode values obtained using DS (0.10 + 0.039 M), (0.25+0.078 M), and (0.50 + 0.078 M) and DI water as feed (298.15 K, cross-flow velocity = 8.55 cm s^{-1}).

3.6 FO desalination performance of Rm-β-CD/oligo([vbim]TFSI)

The FO system was fed with 0.6 M NaCl to simulate the seawater desalination using 0.5 M Rm-β-CD/0.078 M oligo([vbim]TFSI) DS under PRO mode. FO operation time profile reveals the consistent performance of the DS with steady increase in J_v and J_s (**Fig. 6a**). Because the feed has osmolality ~ 1.18 Osmol kg^{-1} [29], the effective gradient ($\Delta\pi$) across the FO membrane would be lower than with DI as feed. For the same reason, NaCl at the feed side would induce concentrative ICP near the support layer of the membrane and would further reduce $\Delta\pi$. These factors explain the lower J_v and J_s values from seawater than from DI as feed (**Fig. 6b**). The effect of reduced gradient was more remarkable on the J_v hence, J_s/J_v from seawater was higher than from DI as

feed. Using a single TFC FO membrane, 0.5 M Rm-β-CD/0.078 M oligo([vbim]TFSI) was able to produce an average $J_v \sim 4.30$ $Lm^{-2}h^{-1}$, $J_s \sim 4.6 \times 10^{-3}$ $molm^{-2}h^{-1}$, and $J_s/J_V \sim 1.07 \times 10^{-3}$ $molm^{-2}h^{-1}$ over 5 cycled FO runs (**Fig. 6c**). There was a slight decline in J_v and an increase in J_s but both parameters stabilized after the 3rd cycle (**Fig. 6d**). Similarly, the J_s/J_V values stabilized from the 4th cycle onwards. Thus, Rm-β-CD/oligo([vbim]TFSI) is a reliable DS for consistent FO performance.

Desalination results reveal that Rm-β-CD/oligo([vbim]TFSI) outperformed numerous DS reported literature (**SI Table S4**) including inorganic solutes [82, 87], organic compounds [42], thermo-responsive organic DS [14,29,31,33,42,88,89], and composite hydrogels [90 - 95]. Overall, Rm-β-CD/oligo([vbim]TFSI) complex was able to successfully desalinate simulated seawater (0.6 M NaCl).

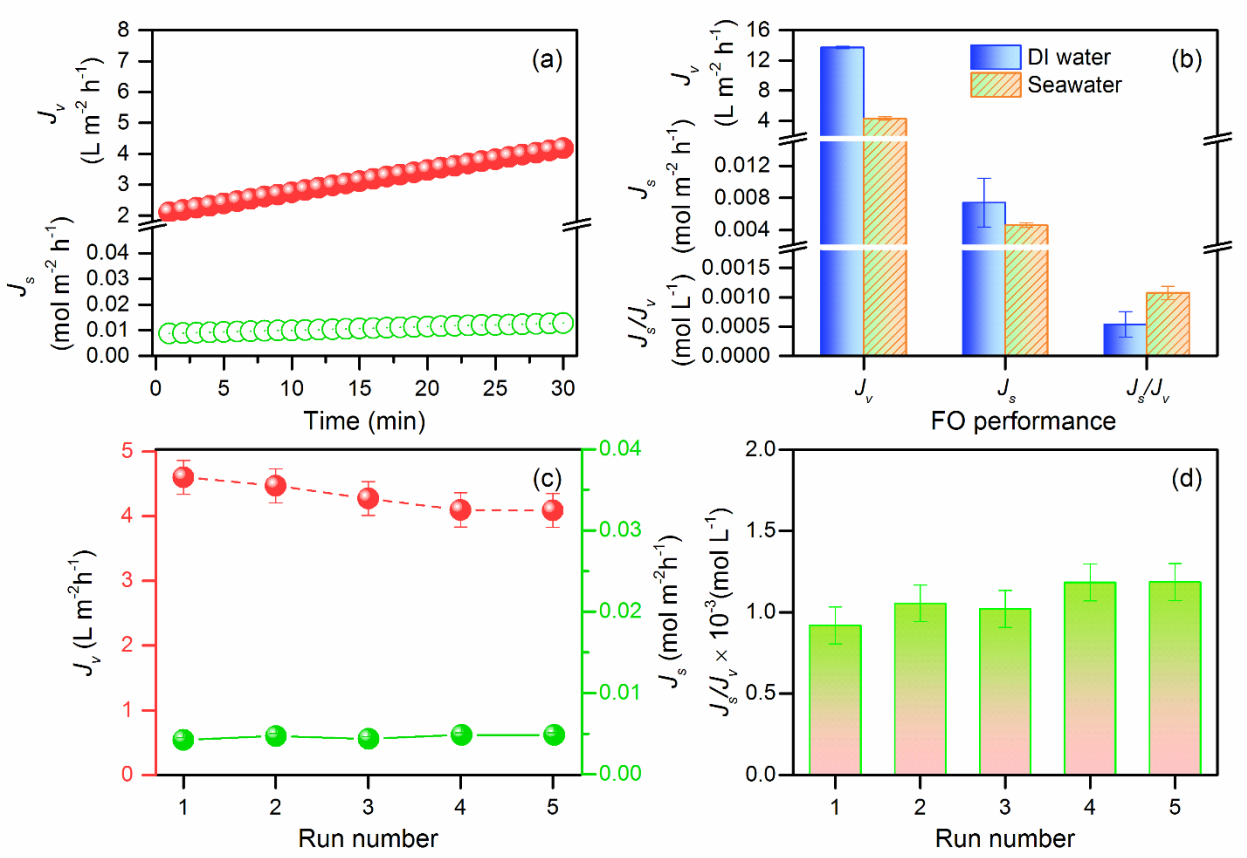

Fig. 6. Performance of 0.50 M Rm-β-CD/0.078 M oligo([vbim]TFSI) for seawater desalination application under PRO mode: (a) time profiles of J_v and J_s values (Feed: 0.6 M NaCl as simulated seawater); (b) average J_v, J_s, and J_s/J_v values obtained using simulated seawater (0.6 M NaCl) and DI water as feed; (c) J_v and J_s (d) J_s/J_v values from repeated desalination FO runs against 0.6 M NaCl as feed under PRO mode (298.15 K, cross-flow velocity= 8.55 cm s^{-1}).

3.7 Recovery and re-use of Rm-β-CD/oligo([vbim]TFSI)

3.7.1 Thermal precipitation for bulk DS recovery

After FO desalination run, the spent DS Rm-β-CD/oligo([vbim]TFSI) is diluted by the permeated water from the FS. Since FO was operated at $T = 25^oC < T_c$, oligo([vbim]TFSI) remains complexed with Rm-β-CD thus the spent DS maintains a clear homogeneous state (**Fig. 7a)**. Results from DLS reveal that the molecular dispersion of the complex has a hydrodynamic diameter d_h = 3 nm (**Fig. 7b**). Thermal precipitation was carried out to recover the bulk draw solutes. Transmittance heating curve of the spent DS reveal that the T_c = 29ºC was not significantly altered by the permeated water (**Fig. 7c**). Heating the spent DS near its T_c ~ 28 ºC triggers the de-complexation of oligo([vbim]TFSI) from Rm-β-CD. The released oligo([vbim]TFSI) precipitates as its "free" form is insoluble in water. Its dispersion size slightly increased to d_h ~ 16 nm **(Fig. 7b)**, rendering the spent DS highly turbid **(Fig.7d)**. The suspension size is drastically increased to d_h = 460 nm when the TP temperature is set at T = 30 ºC but further increase to T = 40 ºC showed marginal improvement in precipitate size with d_h = 520 nm. These results demonstrate that Rm-β-CD/oligo([vbim]TFSI) has very high de-mixing efficiency wherein its TP temperature can be set near its T_c not to induce precipitation but also to facilitate particulate aggregation. This was further evidenced by the efficient phase separation at $T \geq 30$ (**Fig. 7e**). Thus, the TP temperature for the spent DS was set at $T = 30^oC$ to ensure convenient settling of the aggregates with minimal E_{TP}. The mechanism involved in bulk TP recovery of the draw solutes was further elucidated as ~95 %

of the de-complexed Rm-β-CD and oligo([vbim]TFSI) were recovered (**Fig. 7f**). Analysis of the settled DS via FTIR reveals high signals for both Rm-β-CD and oligo([vbim]TFSI **(SI Fig. S8),** suggesting that majority of Rm-β-CDs were removed along with the oligo([vbim]TFSI). Analysis of the DS supernatant via TOC analysis also confirms that it only contained ~ 30 g L^{-1} residual draw solutes from ~ 651 g/L initial DS concentration. From these results, a proposed phase separation mechanism (**Fig. 7e**) highlights the aggregative or coagulative property of de-complexed oligo([vbim]TFSI). At T slightly above T_c, majority of the Rm-β-CDs were physically entrapped within the chains of the "free" oligo([vbim]TFSI as the latter precipitates from water. Thus, bulk draw solute recovery was possible although the host-guest molecules were in their de-complexed states. This particular phase separation mechanism is quite unique and rarely encountered for thermal recovery of host-guest draw solutes in FO process.

The thermo-regenerability of Rm-β-CD/oligo([vbim]TFSI) was assessed through cycled FO-TP runs (**Fig. 7f**). After TP and sedimentation of Rm-β-CD/oligo([vbim]TFSI) aggregates, the settled draw solute phase has very low moisture content (5.21 ± 1.24 %). Thus, it was collected and directly re-dissolved in water for re-use in the next FO run. Five cycles of operation reveal that TP consistently recovered Rm-β-CD/oligo([vbim]TFSI) at an average of ~ 95% after each FO run. The residual draw solute concentration in the DS supernatant ranged between 20 to 40 g L^{-1}, which is only 3 – 6% of the initial DS concentration. These results demonstrate that Rm-β-CD/oligo([vbim]TFSI) can be effectively re-used as DS through very mild heating, which is only ΔT = 5ºC above the FO operating temperature.

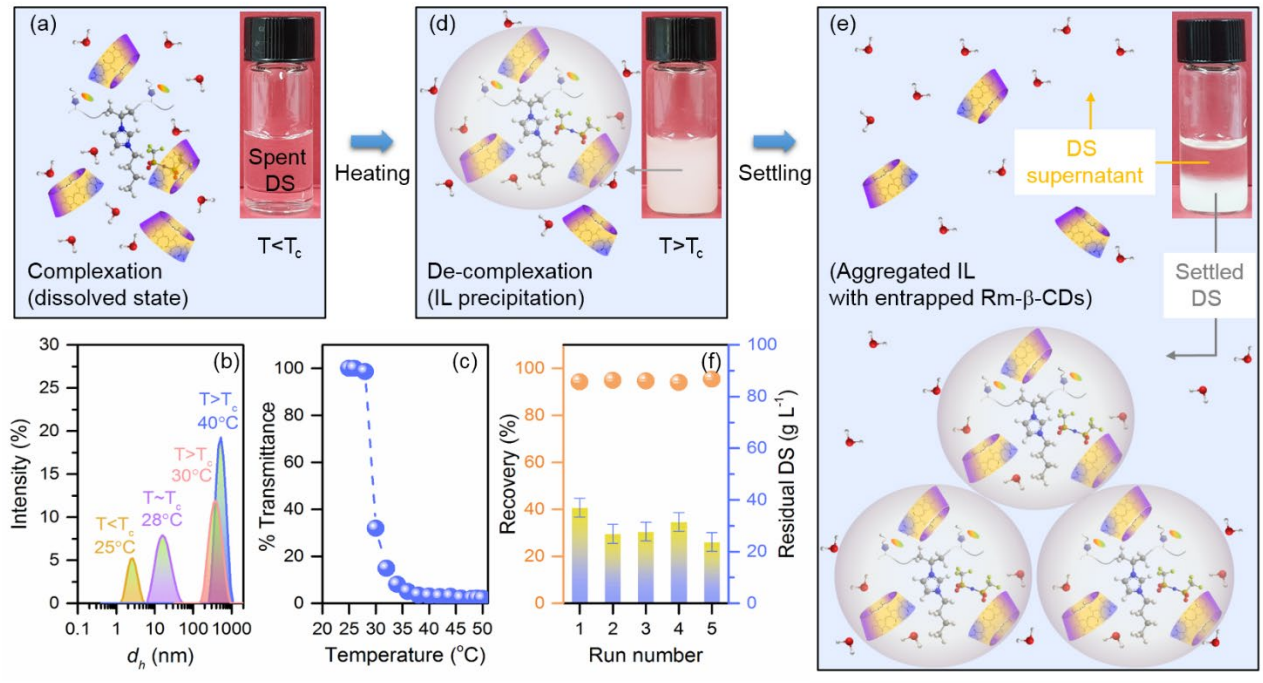

Fig. 7. Thermal recovery of spent Rm-β-CD/oligo([vbim]TFSI): (a) illustration of spent DS in dissolved state at T< T_c ; (b) hydrodynamic diameter (d_h) of Rm-β-CD/oligo([vbim]TFSI) at varied temperature (25 – 40 °C); (c) transmittance during ramped heating of spent Rm-β-CD/oligo([vbim]TFSI) after FO desalination run; (d) illustration of spent DS precipitation at T >T_c; (e) illustration of DS settling after precipitation; (f) % DS recovery and residual DS in water rich supernatant after thermal recovery.

3.7.2 Nanofiltration of DS supernatant and cytotoxicity profile of DS

Removal of residual draw solutes in the DS supernatant was carried out through nanofiltration (NF) to produce high quality effluent. As a final step, the performance of NF was evaluated in terms of water flux (J_w in L m^{-2}h^{-1}), solute rejection (% *SR*) and permeate concentration (C_p in mg L^{-1}). A single NF membrane was repeatedly used five times to demonstrate the consistent removal of the residual draw solutes. On the average, the commercial NF was able to produce J_w ~10.36 ± 0.87 L m^{-2}h^{-1} with ~ 99.3 *% SR* (**Fig. 8a**). This indicates that only 42 % of the FO membrane area is needed for the NF to achieve water permeate balance (i.e. similar flux from FO to NF). The permeate has an average concentration of C_p = 117 ± 8.31 mg L^{-1} (**Fig. 8b**), which is way below

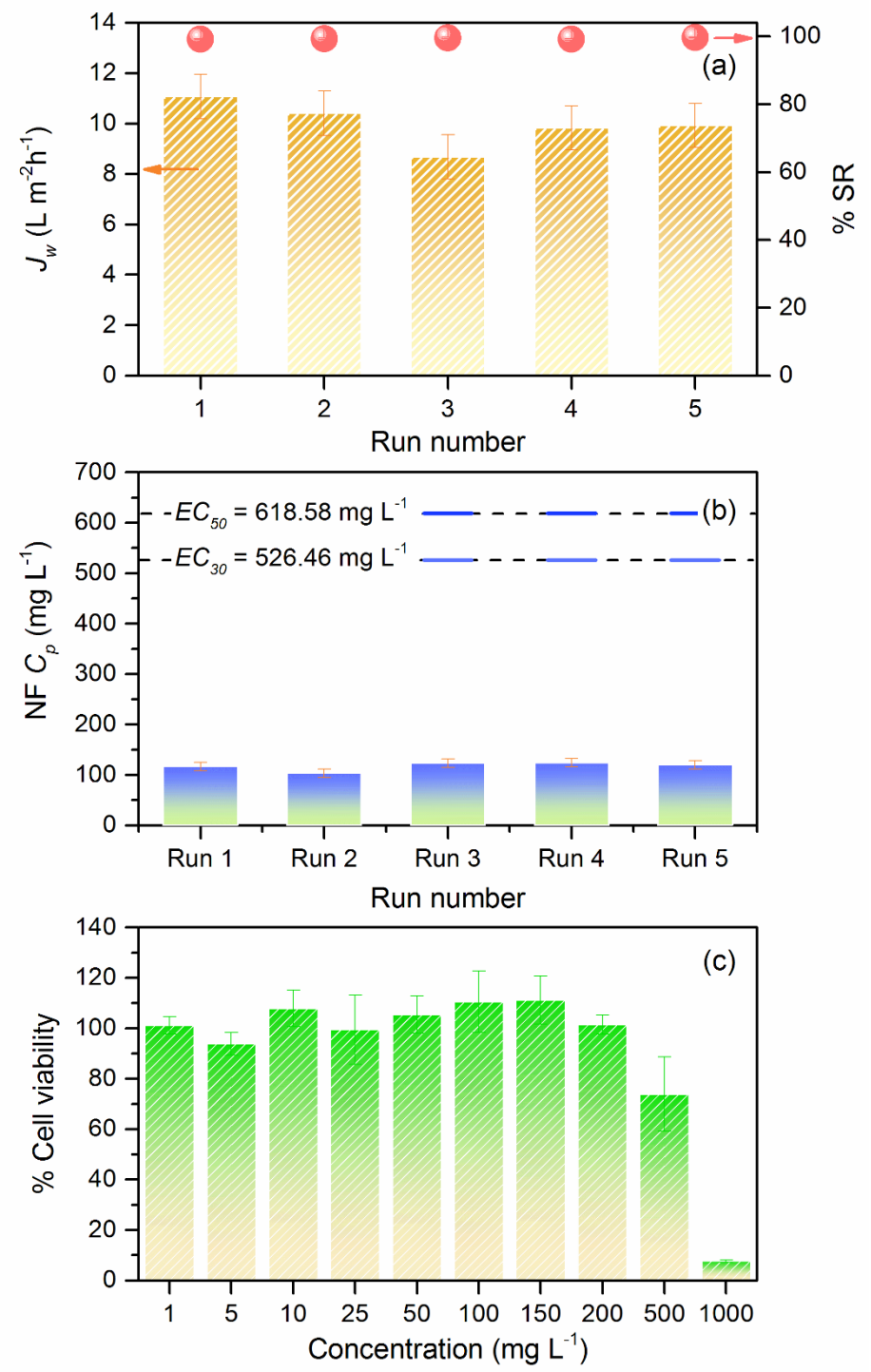

Fig. 8. Residual DS recovery and water purification using nanofiltration (NF): (a) water flux (J_w) and DS rejections *(%SR*); (c) permeate concentration (C_p); (d) % cell viability relative to control from MTT assay.

the calculated EC_{50} and EC_{30} as concentration limits for Rm-β-CD/oligo([vbim]TFSI) derived from the MTT assay results as *in vitro* cytotoxicity test for Rm-β-CD/oligo[vbim]TFSI solution (**SI p. S9**). As shown, ~ 100 % of the cells remained viable up to 200 mg L^{-1} of Rm-β-CD/oligo[vbim]TFSI after 72 h treatment (**Fig. 8c**) and > 70% at ~ 500 mg L^{-1}. A dose-response (D-R) model (**SI p. S9−S10**) was used to determine the values of EC_{50} = 618.58 mg L^{-1} and EC_{30} = 526.46 mg L^{-1} **(SI Fig. S9).** The latter concentration limit is the standard set by the international organization for standardization (ISO 10993-5-2009) [96]. Thus, the measured C_p values indicates that the produced water is safe for consumption [96-98]. Thus, NF can be integrated with FO system using Rm-β-CD/oligo([vbim]TFSI) thermo-recyclable complex as draw solutes for water production.

3.8 Energy requirements and costs to operate the FO-NF with thermal regeneration

Cost estimates were limited on DS preparation and energy requirements for FO, TP and NF operation. Expenses related to other material requirements and construction are not easy to account hence were not included. Survey on current chemical prices reveal that one liter of the DS with 0.5 M Rm-β-CD/0.078 M oligo([vbim]TFSI) would cost $ 2.82, inclusive of the expenses for the starting materials of oligo([vbim]TFSI) synthesis, β-CD and reagents for the methylation of β-CD (**SI Table S5**). The cost of Rm-β-CD/oligo([vbim]TFSI) is comparable with NH_4HCO_3 [9], $KHCO_3$ [9], KCl [9], and $CaCl_2$ [9], and even cheaper than others [99] like $Ca(NO_3)_2$ [9], N, N-dimethylcyclohexamine [100], tri-methylamine [80], PSSS-PINIPAM [35], PAA-Na [101], ferric and cobaltous hydroacid complexes [15], and carbonized quantum dots [102]. With its thermo-responsive property, the regenerability of Rm-β-CD/oligo([vbim]TFSI) through TP is an advantage over other conventional organic and inorganic draw solutes, which are low-cost but

difficult to recycle [9,16,77,81,85, 103]. Thus, expenses related with Rm-β-CD/oligo([vbim]TFSI) preparation can be considered as a capital investment ($2,819 m^{-3} DS) since it can be used for long-term operation.

As mentioned earlier, FO alone requires minimal energy ~ 0.25 kWh m^{-3} mainly for the circulation of streams at both sides of the membrane [10, 17, 35, 104, 105]. Meanwhile, the supernatant DS which contains residual Rm-β-CDs (~ 20 − 40 g L^{-1}g/L) has only 1.45 bar of osmotic pressure. Thus, low applied pressure is needed to filter the DS supernatant using NF. Nonetheless, the NF system was applied with 10 bars to produce J_w ~10.36 ± 0.87 L $m^{-2}h^{-1}$. From literature, the energy needed is estimated to be ~ 0.44 kWh m^{-3} [106].

The thermal energy requirement for heating the spent DS from 25 ºC to 30 ºC was finally estimated using the c_p of the spent DS at 25 ºC derived from DSC analysis (**SI Fig. S10)**. Heating the DS solution to only 5 ºC above the FO operating temperature is a significant improvement among thermo-responsive draw solutes for FO reported in literature. For instance, phase separation is typically achieved by heating BuMP to 31.7 ºC [30], PNiPAM-SA to 45 ºC [14], P($MT_{20}EO_{80}$) to 51 ºC [34], 15SN to 45 ºC [35], PSSP11 to 47 ºC [32], [N4444]2,4,6-$MeSO_3$ to 57 ºC [36], [P444]TsO to 57 ºC [37], GE_7B_3 to 60 ºC [38], and PNA-10 to 70 ºC [39] . Thus, minimal thermal energy requirement for these materials are ~ 7.7 − 29 KWh m^{-3} [35-37]. Meanwhile, the TP for Rm-β-CD/oligo([vbim]TFSI) in spent DS needs only 4.85 KWh m^{-3} (**SI Table S6**), which is only ~16.72 − 62.42 % of those previously reported [35-37]. Taking into account the major process steps, FO-NF with TP for Rm-β-CD/oligo([vbim]TFSI) regeneration requires only 5.54 kWh m^{-3}. The total energy requirement in the current system is a significant improvement from other reported systems like FO-MD, which typically require a total of ~ 8.2 − 29. 5 kWh m^{-3} [17, 35-

37], FO-NF with TP using LCST-type of DS requiring higher temperatures approaches ~ 8.39 kWh m^{-3} [36], or FO-RO with TP using LCST-type of DS requiring higher temperatures ~ 9.95 kWh m^{-3} [36], FO-with evaporation ~ 110 kWh m^{-3} [19- 21], and FO-magnetic field for magnetic draw solute recovery ~1870 kWh m^{-3} [8].

Based on the current energy price of $ 0.076 per kWh, the operation cost would be $ 0.42 m^{-3} of treated water for FO-NF with TP for LCST Rm-β-CD/oligo([vbim]TFSI) draw solutes (**SI Table S7)** [107]. The price is within the range of RO desalination systems with 2 – 10 kWh m^{-3} energy requirement and estimated costs of $ 0.152 – 0.760 m^{-3} [35,40,41]. It has always been suggested that using low-grade waste heat (LGWH) in TP could further reduce the cost associated with heating the spent DS. Using LGWH would further reduce the cost to only 32.7% of the original estimated heating cost [34,35,108]. Thus, the operation cost could be further reduced to only $ 0.172 m^{-3} for FO-NF with TP (**SI Table S7**). These estimates suggest the promising application of Rm-β-CD/oligo([vbim]TFSI) as effective thermo-regenerable host-guest draw solutes in FO process for seawater desalination TP for its bulk recovery and NF for residual draw solute removal and high quality water effluent production.

4. Conclusions

The potential of host-guest inclusion complexes Rm-β-CD/oligo([vbim]TFSI) as draw solutes is first reported. Rm-β-CD/oligo([vbim]TFSI) was able to efficiently provide the needed FO performances for seawater desalination as reflected by their consistent J_v at reasonable levels, negligible J_s and very low J_s/J_v. The complex draw solute offers the advantage of LCST tunability with high de-mixing efficiency which significantly reduced the heat energy requirement during thermal precipitation for its bulk recovery. Subsequent nanofiltration conveniently produces non-

toxic high quality effluents as it only required low pressure to sieve out residual solutes from the supernatant. Energy consumption estimates reveal that the mild heating requirement of the spent DS has rendered the entire process of FO-NF with thermal precipitation for bulk solute recovery as a feasible alternative to conventional RO. Overall results demonstrate that host-guest inclusion complexes of Rm-β-CD/oligo([vbim]TFSI) belongs to a new class of draw solutes that could pave the way towards advancement of FO desalination technology.

5. Acknowledgement

This research was supported by the National Research Foundation of Korea (NRF) under the Ministry of Science and ICT (2017R1A2B2002109 and 2020R1A2C1003560), Basic Science Research Program through the Ministry of Education (2019R1I1A1A01058207 and 2020R1A6A1A03038817) and by the Korea Institute of Technology Evaluation and Planning (KETEP) funded by the Ministry of Trade, Industry & Energy (MOTIE 20194010201750); by the Australian Research Council (ARC) through the ARC Research Hub for Energy-efficient Separation (IH170100009).

References

1. M. Elimelech, W.A. Phillip, The future of seawater desalination: energy, technology, and the environment, Science 333 (2011) 712-717.
2. A.D. Khawaji, I.K. Kutubkahanah, J. Wie, Advances in seawater desalination technologies, Desalination 221 (2008) 47-49.
3. A. Achilli, T.Y. Cath, A.E. Childress, Power generation with pressure retarded osmosis: An experimental and theoretical investigation, J. Membr. Sci., 343 (2009) 42-52.
4. M.J. Park, R.R. Gonzales, A. Abdel-Wahab, S. Phuntsho, H.K. Shon, Hydrophilic polyvinyl alcohol coating on hydrophobic electrospun nanofiber membrane for high

performance thin film composite forward osmosis membrane, Desalination 426 (2018) 50-59.

5. J. Ren, J.R. McCutcheon, A new commercial biomimetic hollow fiber membrane for forward osmosis, Desalination 442 (2018) 44-50.
6. Q. Ge, M. Ling, T.-S. Chung, Draw solutions for forward osmosis processes: Developments, challenges, and prospects for the future, J. Membr. Sci. 444 (2013) 225-237.
7. Y. Cai, X. Hu, A critical review on draw solutes development for forward osmosis, Desalination 391 (2016) 16-29.
8. N.M. Mazlan, D. Peshev, A.G. Livingston, Energy consumption for desalination: a comparison of forward osmosis with reverse osmosis, and the potential for perfect membranes, Desalination 377 (2016) 138-151.
9. A. Achilli, T.Y. Cath, A.E. Childress, Selection of inorganic-based draw solutions for forward osmosis applications, J. Membr. Sci. 364 (2010) 233-241.
10. R.L. McGinnis, M. Elimelech, Energy requirement of ammonia-carbon dioxide forward osmosis desalination, Desalination 207 (2007) 370-382.
11. K. Lutchmiah, L. Lauber, K. Roest, D.J.H. Harmsen, J.W. Post, L.C. Rietveld, J.B. van Lier, E.R. Cornelissen, Zwitterions as alternative draw solutions in forward osmosis for application in wastewater reclamation, J. Membr. Sci. 460 (2014) 82-90.
12. Q. Ge, T.-S. Chung, Hydroacid complexes: A new class of draw solutes to promote forward osmosis (FO) processes, Chem. Commun. 49 (2013) 8471-8473.
13. Q. Long, G. Qi, Y. Wang, Synthesis and application of ethylenediamine tetraproponic salt as a novel draw solute for forward osmosis application, AIChE J. 61 (2015) 1309-1321.
14. R. Ou, Y. Wang, H. Wang, T. Xu, Thermo-sensitive polyelectrolytes as draw solutions in forward osmosis process, Desalination 318 (2013) 48-55.
15. Q. Ge, F. Fu, T.-S. Chung, Ferric and cobaltous hydroacid complexes for forward osmosis (FO) processes, Water Res. 58 (2014) 230–238.
16. S.K. Yen, F.M. Haja N., M. Su, K.Y. Wang, T.-S. Chung, Study of draw solutes using 2-methylimadazole-based compounds in forward osmosis, J. Membr. Sci. 364 (2010) 242-252.
17. H.G. Zeweldi, L.A. Lumjico, A.P. Bendoy, H.-S. Kim, M.J. Park, H.K. Shon, E.M. Johnson,

H. Lee, W.-J. Chung, The potential of monocationic imidazolium-, phosphonium-, and ammonium-based hydrophilic ionic liquids as draw solutes for forward osmosis, Desalination 444 (2018) 94-106.

18. Q. Chen, Q. Ge, W. Xu, W. Pan, Functionalized imidazolium ionic liquids promote seawater desalination through forward osmosis, J. Membr. Sci 574 (2019) 10-16.
19. J.R. McCutcheon, R.L. McGinnis, M. Elimelech, A novel ammoniacarbon dioxide forward (direct) osmosis desalination process, Desalination 174 (2005) 1–11.
20. J.R. McCutcheon, R.L. McGinnis, M. Elimelech, Desalination by ammonia-carbon dioxide forward osmosis: influence of draw and feed solution concentrations on process performance, J. Membr. Sci. 278 (2006) 114-123.
21. M. Cho, S.H. Lee, D. Lee, D.P. Chen, I.-C. Kim, M.S. Diallo, Osmotically driven membrane processes: exploring the potential of branched polyethyleneimine as draw solute using porous FO membranes with NF separation layers, J. Membr. Sci. 511 (2016) 278-288.
22. J.E. Kim, S. Phuntsho, L. Chekli, J.Y. Choi, H.K. Shon, Environmental and economic assessment of hybrid FO-RO/NF system with selected inorganic draw solutes for the treatment of mine impaired water, Desalination 429 (2018) 96-104.
23. T.Y. Cath, A.E. Childress, M. Elimelech, Forward osmosis: Principles, applications, and recent developments. J. Membr. Sci. 281 (2006) 70–87.
24. T.-S. Chung, X. Li, R.C. Ong, Q. Ge, H. Wang, G. Han, Emerging forward osmosis (FO) technologies and challenges ahead for clean water and clean energy applications, Curr 1(2012) 246-257.
25. Q. Long, Y. Jia, J. li, J. Yang, F. Liu, J. Zheng, Recent advance on draw solute development in forward osmosis, Processes 6 (2018) 165.
26. Q. Ge, J. Su, T.-S. Chung, G. Amy, Hydrophilic superparamagnetic nanoparticles: synthesis, characterization, and performance in forward osmosis processes, Ind. Eng. Chem. Res. 50 (2011) 382-388.
27. Y. Cai, W. Shen, R. Wang, W.B. Krantz, A.G. Fane, X. Hu, CO_2 switchable dual responsive polymers as draw solutes for forward osmosis desalination, Chem. Commun. 49 (2013) 8377-8379.
28. Y. Zhong, X. Feng, W. Chen, X. Wang, K.-W. Huang, Y. Gnanou, Z. Lai, Using UCST

ionic liquids as draw solute in forward osmosis to treat high-salinity water, Environ. Sci. Technol. 50 (2016) 1039-1045.

29. Y. Cai, W. Shen, J. Wei, T.H. Chong, R. Wang, W.B. Krantz, A.G. Fane, X. Hu, Energy-efficient desalination by forward osmosis using responsive ionic liquid draw solutes, Environ. Sci.: Water Res. Technol. 1 (2015) 341-347.
30. A. Inada, T. Takahashi, K. Kumagai, H. Matsuyama, Morpholine derivatives as thermoresponsive draw solutes for forward osmosis desalination, Ind. Eng. Chem. Res. 58 (2019) 12253-12260.
31. D. Nakayama, Y. Mok, M. Noh, J. Park, S. Kang, Y. Lee, Lower critical solution temperature (LCST) phase separation of glycol ethers for forward osmotic control, Phys. Chem. Chem. Phys. 16 (2014) 5319-5325.
32. J.-j Kim, H. Kang, Y.-S. Choi, Y.A. Yu, J.-C. Lee, Thermo-responsive oligomeric poly (tetrabutylphosphonium styrenesulfonate)s as draw solutes for forward osmosis (FO) applications, Desalination 381 (2016) 84-94.
33. K.L. Tu, G.P. Simon, H. Wang, Fast-responsive monolithic hydrogels as draw agent for forward osmosis membrane process, Sep. Sci. Technol. 16 (2017) 2583-2590.
34. J.-j Kim, J.-S. Chung, H. Kang, Y.A. Yu, W.J. Choi, H.J. Kim, J.-C. Lee, Thermo-responsive copolymers with ionic group as novel draw solutes for forward osmosis processes, Macromol. Res. 22 (2014) 963-970.
35. D. Zhao, P. Wang, Q. Zhao, N. Chen, X. Lu, Thermoresponsive copolymer-based draw solution for seawater desalination in a combined process of forward osmosis and membrane distillation, Desalination 348 (2014) 26-32.
36. H.G. Zeweldi, A.P. Bendoy, M.J. Park, H.K. Shon, H.-S. Kim, E.M. Johnson, S.P. Lee, W.-J. Chung, G.M. Nisola, Tetrabutylammonium 2,4,6-trimethylbenzenesulfonate as an effective and regenerable thermo-responsive ionic liquid drawing agent in forward osmosis for seawater desalination, Desalination 495 (2020)114635.
37. H.G. Zeweldi, A.P. Bendoy, M.J. Park, H.K. Shon, H.-S. Kim, E.M. Johnson, H. Kim, W.-J. Chung, G.M. Nisola, Forward osmosis with direct contact membrane distillation using tetrabutylphosphonium p-toluenesulfonate as an effective and safe thermo-recyclable osmotic agent for seawater desalination, Chemosphere 263 (2021) 128070.
38. A. Inada, K. Yumiya, T. Takahashi, K. Kumagai, Y. Hashizume, H. Matsuyama,

Development of thermoresponsive star oligomers with a glycerol backbone as the draw solute in forward osmosis process. J. Membr. Sci. 574 (2019) 147-153.

39. Y. Wang, H. Yu, R. Xie, K. Zhao, X. Ju, W. Wang, Z. Liu, L. Chu, An easily recoverable thermo-sensitive polyelectrolyte as draw agent for forward osmosis process, Chin. J. Chem. Eng. 24 (2016) 86-93.
40. R. Dashtpour, S.N. Al-Zubaidy, Energy efficient reverse osmosis desalination process. J. Environ. Sci. Dev. 3 (2012) 339-345.
41. I.C. Escobar, A. Schäfer, Sustainable water for the future: water recycling versus desalination. Elesevier 2 (2010) 1-416.
42. M.A.M. Abdullah, M.S. Man, P.S. Nyan, S.M. Saufi, S.B. Abdullah, Potential thermo-responsive ionic liquid as draw solution in forward osmosis application, J. Eng. Sci. Technol. 14 (2019) 1031-1042.
43. E.M.M.D. Valle, Cyclodextrins and their uses: a review, Process Biochemistry 39 (2004) 1033-1046.
44. J. Szejtli, Introduction and general overview of cyclodextrin chemistry, Chem. Rev. 98 (1998) 1743–1753.
45. A.M. Fernandes, B. Schröder, T. Barata, M.G. Freire, J.A.P. Coutinho, Inclusion complexes of ionic liquids and cyclodextrins: Are they formed in the gas phase?, J. Am. Soc. Mass Spectrom. 25 (2014) 852-860.
46. E.A. Zannou, W.H. Streng, V.J. Stella, Osmotic properties of sulfobutylether and hydroxypropyl cyclodextrins, Pharm. Res. 18 (2001) 1226.
47. C.C. Rusa, T.A. Bullions, J.Fox, F.E. Porbeni, X. Wang, A.E. Tonelli, Inclusion compound formation with a new columnar cyclodextrin host, Langmuir 18 (2002) 10016-10023.
48. M.N. Roy, D. Ekka, S. Saha, M.C. Roy, Host-guest inclusion complexes of α and β-cyclodextrin with α-amino acids, RSC. Adv. 4 (2014) 42383-42390.
49. S. Bucatariu, M. Constantin, P. Ascenzi, G. Fundueanu, Poly(lactide-*co*-glycolide)/cyclodextrin (polyethyleneimine) microspheres for controlled delivery of dexamethasone. React Funct Polym. 107 (2016) 46-53.
50. S. Schmitz, H. Ritter, Unusual solubility properties of polymethacrylamides as a result of supramolecular interactions with cyclodextrin, Angew. Chem. Int. Ed. 44 (2005) 5658 – 5661.

51. I. Böhm, K. Isenbügel, H. Ritter, R. Branscheid, U. Kolb, Cyclodextrin and adamantane host-guest interactions of modified hyperbranched poly(ethylene imine) as mimetics for biological membranes, Angew. Chem. Int. Ed. 50 (2011) 7896 -7899.
52. S. Jacob, A.B. Nair, Cyclodextrin complexes: perspective from drug delivery and formulation, Drug Dev Res. 79 (2018) 201-217.
53. V. Bonnet, C. Gervaise, F. D.-Pilard, A. Furlan, C. Sarazin, Cyclodextrin nanoassemblies: a promising tool for drug delivery, Drug Discovery Today 20 (2015) 1120-1126.
54. S. Bucatariu, M. Constantin, P. Ascenzi, G. Fundueanu, Poly(lactide-co-glycolide)/cyclodextrin (polyethyleneimine) microspheres for controlled delivery of dexamethasone. React. Funct. Polym. 107 (2016) 46–53.
55. R. Bhardwaj, R.T. Dorr, J. Blanchard, Approaches to reducing toxicity of parenteral anticancer drug formulations using cyclo-dextrins, J Pharm Sci Technol 54 (2000) 233–9.
56. N. Fujishima, K. Kusaka, T. Umino, T. Urushinata, K. Terumi, Flour based foods containing highly branched cyclodextrins. Japanese Patent JP 136 (2001) 898.
57. L. Holland, G. Rizzi, P. Malton, Cosmetic compositions comprising cyclic oligosaccharides and fragrance. PCT Int Appl WO 67 (1999) 716.
58. RA. Hedges, Industrial applications of cyclodextrins, Chem Rev 98(1998) 2035–44.
59. L. Dufosse, I. Souchon, G. Feron, A. Latrasse, HE. Spinnler, In situ detoxification of the fermentation medium during gamma-decalactone production with the yeast Sporidiobolus salmonicolor, Biotechnol Prog 15 (1999)135–9.
60. S. Amajjahe, H. Ritter, Anion complexation of vinylimidazolium salts and its influence on polymerization, Macromolecules 41 (2008) 716-71.
61. S. Amajjahe, H. Ritter, Supramolecular controlled pseudo-LCST effect of cyclodextrin-complexed poly (ionic liquids), Macromolecules 41, 3250-3253 (2008).
62. K. Beltrop, P. Meister, S. Klein, A. Heckmann, M. Grünebaum, H.-D. Wiemhöferm M. Winter, T. Placke, Does size really matter? New insights into the intercalation behavior of anions into graphite-based positive electrode for dual-ion batteries, Electrochim. Acta. 209 (2016) 44-55.
63. J. Zhao, X. Shen, F. Yan, L. Qiu, S. Lee, B. Sun, Solvent-free ionic liquid/poly(ionic liquid) electrolytes for quasi-solid-state-dye-sensitized solar cells, J. Mater. Chem. 21(2011) 7326-7330.

64. H. He, M. Zhong, B. Adizma, D. Luebke, H. Nulwala, K. Matyjaszewski, A simple and universal gel permeation chromatography (GPC) technique for precise molecular weight characterization of well-defined poly(ionic liquid)s, J. Am. Chem. Soc. 135 (2013) 4227-4230.
65. C.R. Wilke, P. Chang, Correlation of diffusion coefficients in dilute solutions, AIChE J. 1 (1955) 264-270.
66. M.T. Tyn, W.F. Calus, Diffusion coefficients in dilute binary liquid mixtures, J. Chem. Eng. Data. 20 (1975) 106-109.
67. J.O. Valderrama, P.A. Robles, Critical properties, normal boiling temperatures, and acentric factors of fifty ionic liquids, Ind. Eng. Chem. Res. 46 (2017) 1338-1344.
68. M. Bonnet, A. Ouali, J. Kopp, Beef muscle osmotic pressure as assessed by differential calorimetry (DSC), Int. J. Food. Sci., 27 (1992) 399-408.
69. Q.-T. Pham, Z.-H. Yao, Y.-T. Chang, F.-M. Wang, C.-S. Chern, LCST phase transition kinetics of aqueous poly(N-isopropylacrylamide) solution, J Taiwan Inst Chem Eng. 000 (2018) 1-7.
70. J. E. Daw, Measurement of specific heat capacity using differential scanning calorimeter, U.S. Department of Energy National Laboratory, Idaho, 2008.
71. H. He, M. Zhong, B. Adizma, D. Luebke, H. Nulwala, K. Matyjaszewski, A simple and universal gel permeation chromatography (GPC) technique for precise molecular weight characterization of well-defined poly(ionic liquid)s, J. Am. Chem. Soc. 135 (2013) 4227-4230.
72. M. Tarnacka, A. Chrobok, K. Matuszek, D. Neugebauer, R. Bielas, S. Golba, K. Wolnica, M. Dulski, K. Kaminski, M. Paluch, Studies on the radical polymerization of monomeric ionic liquids: nanostructure ordering as a key factor controlling the reaction properties of nascent polymers, Polym. Chem. 7 (2016) 6363-6374.
73. A. Wu, F. Lu, P. Sun, X. Qiao, X. Gao, L. Zheng, Low molecular weight supramolecular iongel based on host-guest interaction, Langmuir 33 (49) (2017) 13982-13989.
74. M.B.– Rogač, M.V. Fedotova, S.E. Kruchinin, M. Klähn, Mobility and association of ions in aqueous solutions: the case of imidazolium based ionic liquids, Phys. Chem. Chem. Phys. 18 (2016) 28594-28605.

75. A. Atahar, M.Y.A. Mollah, M.M. Rahman, M.A.B.H. Susan, Inclusion complexes of cyclodextrins with hydrophobic ionic liquids, J. Incl. Phenom. Macrocycl. Chem. 92 (2018) 301-309.
76. H. Manzoor, M.A. Selam, S. Adham, H.K. Shon, M. Castier, A.A.- Wahab, Energy recovery modeling of pressure-retarded osmosis system with membrane modules compatible with high salinity draw solutes, Desalination 493 (2020) 114624.
77. J.S. Yong, W.A. Phillip, M. Elimelech, Coupled reverse draw solute permeation and water flux in forward osmosis with neutral draw solutes, J. Membr. Sci. 392-393 (2012) 9-17.
78. W.A. Phillip, J.S. Yong, M. Elimelech, Reverse draw solute permeation in forward osmosis: Modeling and experiments, Environ. Sci. Technol. 44 (2010) 5170-5176.
79. G.T. Gray, J.R. McCutcheon, M. Elimelech, Internal concentration polarization in forward osmosis: Role of membrane orientation, Desalination 197 (2006) 1-8.
80. C. Boo, Y.F. Khalil, M. Elimelech, Performance evaluation of trimethylamine–carbon dioxide thermolytic draw solution for engineered osmosis, J. Membr. Sci. 473 (2015) 302-309.
81. S. Phuntsho, H.K. Shon, S. Hong, S. Lee, S. Vigneswaran, A novel low energy fertilizer driven forward osmosis desalination for direct fertigation: Evaluating the performance of fertilizer draw solution. J. Membr. Sci. 375 (2011) 172-181.
82. M. Qasim, F. Mohammed, A. Aidan, N.A. Darwish, Forward osmosis desalination using ferric sulfate draw solute, Desalination 423 (2017) 12-20.
83. M. Guizani, T. Maeda, R. Ito, N. Funamizu, Synthesis and characterization of magnetic nanoparticles as a candidate draw solution for forward osmosis, J. Water Environ. Technol. 16 (2018) 63-71.
84. K.S. Bowden, A. Achilli, A.E. Childress, Organic ionic salt draw solutions for osmotic membrane bioreactors, Bioresour. Technol. 122 (2012) 207-216.
85. K. Lutchmiah, J.W. Post, L.C. Rietveld, E.R. Cornelissen, EDTA: a synthetic draw solute for forward osmosis, Water Sci. Technol. 70 (2014) 1677-1682.
86. J. Kim, J. Kim, J. Lim, S. Hong, Evaluation of ethanol as draw solute for forward osmosis (FO) process of highly saline (waste)water, Desalination 456 (2019) 23-31.
87. J. Duan, E. Litwiller, S.-H. Choi, L. Pinnau, Evaluation of sodium lignin sulfonate as a draw solute in forward osmosis for desert restoration, J. Membr. Sci. 453 (2014) 463-470.

88. J. Park, H. Joo, M. Noh, Y. Namkoong, S. Lee, K.H. Jung, H.R. Ahn, S. Kim, J.-C. Lee, J.H. Yoon, Y. Lee, Systematic structure control of ammonium iodide salts as feasible UCST-type forward osmosis draw solutes for the treatment of wastewater, J. Mater. Chem. A. 6 (2018) 1255-1265.
89. M. Noh, Y. Mok, S. Lee, H. Kim, S.H. Lee, G.-W. Jin, J.-H. Seo, H. Koo, T.H. Park, Y. Lee, Novel lower critical solution temperature phase transition materials effectively control osmosis by mild temperature changes, Chem. Commun. 48 (2012) 3845-3847.
90. D. Li, X. Zhang, J. Yao, G.P. Simon, H. Wang, Stimuli-responsive polymer hydrogels as a new class of draw agent for forward osmosis desalination, Chem. Commun. 47 (2011) 1710-1712.
91. A. Razmjou, M.R. Barati, G.P. Simon, K. Suzuki, H. Wang, Fast deswelling of nanocomposite polymer hydrogels via magnetic field-induced heating for emerging FO desalination, Environ. Sci. Technol. 47 (2013) 6297-6305.
92. Y. Zeng, L. Qiu, K. Wang, J. Yao, D. Li, G.P. Simon, R. Wang, H. Wang, Significantly enhance water flux in forward osmosis desalination with polymer-graphene composite hydrogels as drawing agents, RSC Adv. 3 (2013) 887-894.
93. A. Razmjou, G.P. Simon, H. Wang, Effect of particle size on the performance of forward osmosis desalination by stimuli-responsive polymer hydrogels as draw agent, Chem. Eng. J. 215-216 (2013) 913-920
94. X. Fan, H. Liu, Y. Gao, Z. Zou, V.S.J. Craig, G. Zhang, G. Liu, Forward-osmosis desalination with poly (ionic liquid) hydrogels as smart draw agents, Adv. Mater. 28 (2016) 4156-4161.
95. H. Cui, H. Zhang, M. Yu, F. Yang, Performance evaluation of electric-responsive hydrogels as draw agent in forward osmosis desalination, Desalination 426 (2018) 118-126.
96. International standard ISO100993-5-2009, Biological evaluation of medical devices Part 5: Tests for invitro cytotoxicity.
97. M. O'Donovan, A critique of methods to measure cytotoxicity in mammalian cell genotoxicity assays, Mutagenesis 27 (2012) 615-621.
98. L. Braz, A. Grenha, D. Ferreira, A.M.R.d. Costa, C. Gamazo, B. Sarmento, Chitosan/sulfated locust bean gum nanoparticles: In vitro and in vivo evaluation towards an application in oral immunization, Int J biol Macromol 96 (2017) 786-797.

99. D.J. Johnson, W.W. Suwaileh, A.W. Mohammed, N. Hilal, Osmotic's potential: an overview of draw solutes for forward osmosis, Desalination 434 (2018) 100-120.
100. M.L. Stone, C. Rae, F.F. Stewart, A.D. Wilson, Switchable polarity solvents as draw solutes for forward osmosis, Desalination 312 (2013) 124-129.
101. Q. Ge, J. Su, G.L. Amy, T.-S. Chung, Exploration of polyelectrolytes as draw solutes in forward osmosis processes, Water Res. 46 (2012) 1318–1326.
102. C.X. Guo, D. Zhao, Q. Zhao, P. Wang, X. Lu, Na+-functionalized carbon quantum dots: a new draw solute in forward osmosis for seawater desalination, Chem. Commun. 50 (2014) 7318–7321.
103. N.Q. Trung, L.V. Nhan, P.T.P. Thao, L.T. Giang, Novel draw solutes of iron complexes easier recovery in forward osmosis process, J. Water. Reuse. Desal. (2018) 244-250.
104. S. Zou, H. Yuan, A. Childress, Z. He, Energy consumption by recirculation: a missing parameter when evaluation forward osmosis, Environ. Sci. Technol. 50 (2016) 6827–6829.
105. A. Haupt, A. Lerch, Forward osmosis application in manufacturing industries: A short review, Membranes 8 (2018) 47.
106. H. Dach. Comparison of nanofiltration and reverse osmosis processes for a selective desalination of brackish water feeds. Engineering Sciences [physics]. Université d'Angers, 2008. English.
107. South Korea electricity prices, GlobalPetrolPrices.com, https://www.globalpetrolprices.com/South-Korea/electricity_prices/. Accessed 11 July 2020.
108. M. Langan, K. O'Toole, A new technology for cost-effective low-grade waste heat recovery, Energy Procedia. 123 (2017)188-195.